Elsevier Editorial System(tm) for Minerals Engineering

Manuscript Draft

Manuscript Number: MINE-D-19-00634R1

Title: Model Predictive Control of a Rotary Kiln for Fast Electric Demand Response

Article Type: VSI: Computational Modelling '19

Keywords: Ancillary Services; Rotary Kiln; Model Predictive Control; Dynamic Optimization; Steady-state Optimization; Calcination

Corresponding Author: Dr. Kody Merlin Powell, Ph.D.

Corresponding Author's Institution: The University of Utah

First Author: Derek Machalek

Order of Authors: Derek Machalek; Kody M Powell, PhD

Manuscript Region of Origin: USA

Abstract: Rotary kilns require large fans to induce drafts to support transformation of minerals. If fan controls can be modified to respond to rapid changes in electric demand, they can become valuable grid assets. Due to their considerable thermal inertia, kilns and the associated fans are traditionally operated continuously in a steady manner to avoid process disruption. However, advanced process control, such as model predictive control (MPC) can allow for the rigid process to be operated flexibly. Ultimately the flexible process can respond to grid demand requirements by ramping the induced draft fan. Process disturbances generated by a quick change in the kiln air flow rate are buffered by adjusting kiln operations using MPC. In this work, a through, dynamic kiln model was developed. On top of the model, a novel MPC algorithm is presented which leverages kiln rotation rate, stone feed rate, and coal feed rate to ensure successful calcination of limestone while the kiln simultaneously plays a crucial role in electric grid regulation. Four scenarios were explored, long and short term duration of both up and down regulation. The MPC algorithm reduced the number of hours of poor stone quality production to 0 during smart grid participation. The economic penalty of the grid responses was reduced by at least 65% using MPC, compared to steady-state optimized operation. For short-term participation, less than two hours, the MPC algorithm would reduce economic penalties by at least 77%. Minimized economic penalties and high stone quality improve the feasibility of smart grid participation.

Acknowledgement: This material is based upon work supported by the U.S. Department of Energy's Office of Energy Efficiency and Renewable Energy (EERE) under the Advanced Manufacturing Office Award Number DE-EE0007712.

Highlights (for review)

- A methodology to leverage a large thermal process as a smart grid asset
- Construction of a novel dynamic model of a limestone calcining rotary kiln
- Steady-state optimization of a rotary kiln with and without air flow rate constraints
- Development of a novel model predictive control algorithm used to reduce poor quality product production to 0% through operational transitions for the smart grid
- Reduction in economic penalties for smart grid participation by 77% for short term participation

Model Predictive Control of a Rotary Kiln for Fast Electric Demand Response

Derek Machalek and Kody M. Powell

University of Utah, Salt Lake City, Utah, USA

Abstract

Rotary kilns require large fans to induce drafts to support transformation of minerals. If fan controls can be modified to respond to rapid changes in electric demand, they can become valuable grid assets. Due to their considerable thermal inertia, kilns and the associated fans are traditionally operated continuously in a steady manner to avoid process disruption. However, advanced process control, such as model predictive control (MPC) can allow for the rigid process to be operated flexibly. Ultimately the flexible process can respond to grid demand requirements by ramping the induced draft fan. Process disturbances generated by a quick change in the kiln air flow rate are buffered by adjusting kiln operations using MPC. In this work, a through, dynamic kiln model was developed. On top of the model, a novel MPC algorithm is presented which leverages kiln rotation rate, stone feed rate, and coal feed rate to ensure successful calcination of limestone while the kiln simultaneously plays a crucial role in electric grid regulation. Four scenarios were explored, long and short term duration of both up and down regulation. The MPC algorithm reduced the number of hours of poor stone quality production to 0 during smart grid participation. The economic penalty of the grid responses was reduced by at least 65% using MPC, compared to steady-state optimized operation. For short-term participation, less than two hours, the MPC algorithm would reduce economic penalties by at least 77%. Minimized economic penalties and high stone quality improve the feasibility of smart grid participation.

Keywords: Ancillary Services, Rotary Kiln, Model Predictive Control, Dynamic Optimization, Steady-state Optimization, Calcination

1. Introduction

Mineral processing is electrically intensive (Votteler & Brent, 2016). The sector consumes 6.2% of the electricity in the world (Holmberg *et al.* , 2017). This makes

mineral processing facilities candidates to help regulate the grid.

The importance of grid regulation is rising as renewable energy continues to penetrate into the grid (Aghaei & Alizadeh, 2013). Renewable energy sources such as solar and wind are notoriously intermittent (Strbac, 2008). The rise and fall of power generation from these sources creates power production and demand mismatch, which requires active grid management to stabilize (Yu & Hong, 2016; Sheha & Powell, 2018).

While grid regulation is often a problem thrust upon energy suppliers, the best solutions involve both supply and demand side management (DSM) of the grid (Alizadeh *et al.* , 2016). Mineral processing facilities can play a crucial role in DSM. DSM research at mineral processing facilities has primarily focused on peripheral services such as de-watering processes (De Kock, 2006). However, the major electricity consuming equipment at processing facilities is directly tied to the mineral processing itself (Rodríguez *et al.* , 2005). Rudimentary scheduling changes for mineral processing equipment have also been explored, but this application is limited with facilities operating non-stop (Lidbetter & Liebenberg, 2013).

In order for a facility to play a role in DSM, it must be able to be flexible and adjust how much power it is drawing without adverse impacts on the process (Westberg *et al.* , 2018; Henning *et al.* , 2019). Unfortunately, many mineral processing pieces of equipment have long residence time (minutes to hours) which correspond to long transitions to new steady states (Sosa-Blanco *et al.* , 1999; Njeng *et al.* , 2015). Therefore, disturbances to processes are not immediately quelled, and can disrupt for long periods of time. This manifests itself in the literature where operational optimization focuses on steady-state optimization or minor disturbance handling (Roberts, 1979; Zhengyan *et al.* , 2016; Yang *et al.* , 2010).

Further, the mineral processing optimization focuses on product throughput and completely ignores electrical consumption and costs (Zhengyan *et al.* , 2016; Cambitsis, 2013; Ping *et al.* , 2012). However, the assumption that electrical pricing is negligible may no longer be valid. Real-time pricing with massive energy cost spikes, including negative prices is becoming a reality (Barbour *et al.* , 2014; Faria & Vale, 2011). Beyond electrical pricing schedules, facilities can also be paid to perform ancillary services, where they rapidly increase or decrease power consumption to facilitate grid regulation (Ma *et al.* , 2013).

Ancillary service contracts allow power suppliers to rapidly increase or decrease power supplied to facilities to maintain grid stability (Sortomme & El-Sharkawi, 2012). According to Ma, demand responses from manufacturing facilities to perform ancillary services are better suited to perform this than grid reserves because they do not have delays caused by ramping (Ma *et al.* , 2013).

Because mineral processing facilities have long residence times, reacting to a disturbance caused by a power step up or step down propagates through the system for long periods of time. Therefore, real-time optimization, using one fixed set of operating conditions, is not a viable option to handle the changing disturbance. Instead, dynamic optimization must be used to ensure high quality mineral processing in the face of variable conditions. Dynamic optimization is performed using model predictive control (MPC). MPC starts with a model of the mineral processing facility and then evaluates how different manipulated variables for controlling the facility can be dynamically adjusted in order to ensure high quality product in the face of a disturbance (such a power step up or step down). Fortunately, as sensors and computational power have become less expensive (more cost effective), MPC of complex processes have become increasingly viable.

The mineral processing facility in this paper is a rotary kiln. The rotary kiln performs calcination of limestone to lime as shown in Equation 1.

$$CaCO_3(s) \rightarrow CaO(s) + CO_2(g) \tag{1}$$

The calcination is performed around 1400 K (1127 ^oC) and requires over 0.6 MW of electrical power availability for fan operations. Stone residence times in the kiln are on the order of hours, resulting in drawn out process disturbances, necessitating MPC for the kiln to perform ancillary services. In the case of the rotary kiln, the fan speeds (and corresponding air flow rates) are rapidly increased or decreased based on the ancillary service performed. Four scenarios are explored in this paper to evaluate the viability of a rotary kiln to perform ancillary services. Each scenario is classified by a duration and direction. The duration is either short-term (hours or less) or long-term (indefinite) and the direction is either an increase or decrease in power.

Two MPC algorithm are developed and applied to the rotary kiln model: one for each temporal scenario to demonstrate that the kiln can handle process power disturbances and still generate high quality product.

One key highlight of this paper is the complex, thorough rotary kiln model. The subsequent highlight of this paper is that a manufacturing sector traditionally considered operationally rigid shows potential to operate flexibly. The explored rotary kiln is able to successfully handle each of the four proposed ancillary service scenarios without any loss of product. This illustrates the robust operating potential the facility and sector contain.

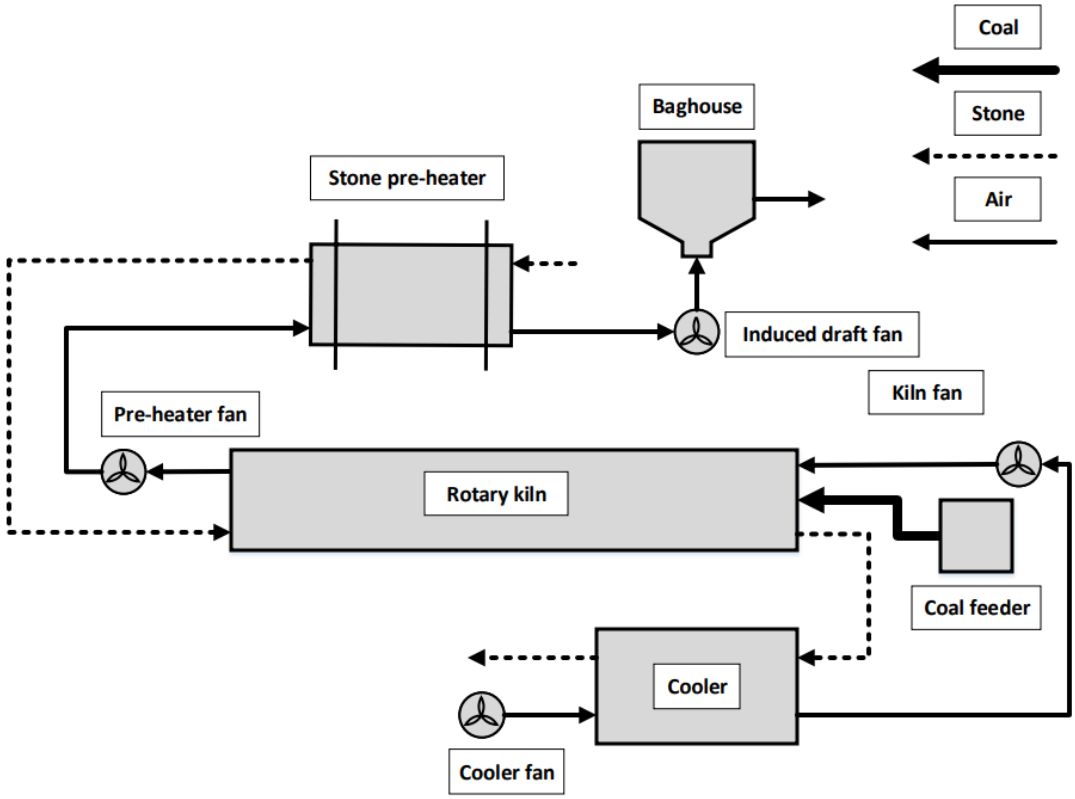

Figure 1: Process flow diagram of the examined rotary kiln facility.

2. Facility Description

This facility is based on a real 100 meter long rotary kiln that processes approximately 80 US tons/hr (20 kg/s) of limestone. While the model is based on an actual operating lime kiln, the facility has chosen to remain anonymous for this study. The key pieces of equipment at the facility are shown in the process flow diagram, Figure 1. Two inch stones (dashed line) are fed through a stone pre-heater, which is pre-heated with the hot air coming out of the rotary kiln. The stones are subsequently sent into the kiln for calcination. The rotation of the kiln and one degree angle of incline (β), as shown in Figure 2, move the stones through the kiln. After calcination the stones are moved to the cooler, where the stone is cooled, while the incoming air is pre-heated as an energy-saving measure.

Air (thin solid line) is primarily pulled through the kiln with the workhorse

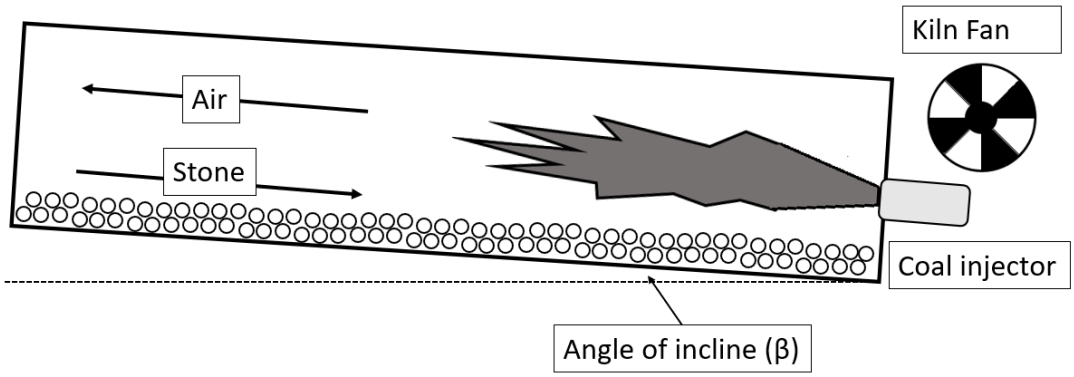

Figure 2: Side view of air and stone flows through the rotary kiln. The coal injector launches coal particles which combust and create a flame.

induced draft fan (1400 kW max), other fans help it along the way. Initially air enters through the stone cooler (air pre-heater) with the cooler fan (185 kW max). The air is then pushed through the rotary kiln with the kiln fan (320 kW), where it enters through the opposite end of the stones as shown in Figure 2. Then it is passed through the stone pre-heater (air-cooler) with the pre-heater fan (140 kW max). All of the fans are setup to operate proportionally to the induced draft fan.

Coal (represented as a thick solid line in Figure 1) is ground and fed into the kiln through the same end as the air. At the air entrance the coal is combusted, resulting in a flame through the first portion of the kiln that provides heat for calcination.

The facility operators have control over the fan power, coal feed rate, stone feed rate, and rotation rate of the kiln. To ensure complete combustion, the flow of oxygen, a function of the fan power, must always be in at least two percent stoichiometric excess of the carbon in the coal. However, maximizing the coal combusted to air flow rate ratio results in the hottest air and highest heat transfer. Therefore, when possible, the kiln is operated at the 2 percent excess of oxygen lower limit.

3. Model

3.1. Electricity Consumption

All of the facility fans are setup to operate proportionally to the induced draft fan, in order to maintain air flow through the baghouse, cooler, rotary kiln, and pre-heater. The air flow rate from the kiln is described by the cube rule to calculate fan power consumption. Based on the facility, the nominal induced draft fan power consumption of 400 kW (584 kW for all fans) corresponds to a volumetric air flow

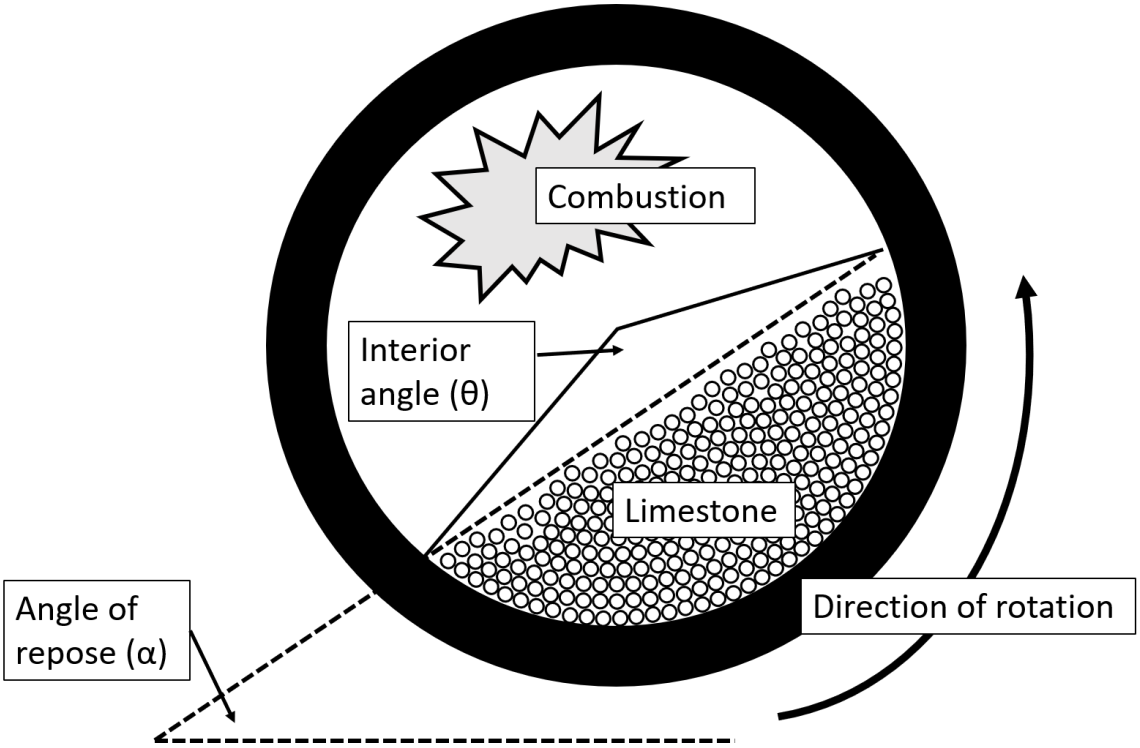

Figure 3: Cross sectional view of rotary kiln including the freeboard area where combustion occurs and limestone bed. Key angles used as modelling parameters are illustrated.

rate of 80 m^3/s. The fan inlet air is assumed to be at ambient air pressure and temperature, therefore the density is constant. As a result, Equation 2, uses the volumetric flow rate ratios to approximate fan power consumption (Stebbins, 1994).

$$P_{fan} = P_{fan,nominal} \frac{\dot{V}_{air}^3}{\dot{V}_{air,nominal}^3} \tag{2}$$

The coal crusher power consumption is linearly proportional to the coal flow rate, and is based on the nominal power values of 140 kW for a coal flow rate of 6.8 kg/s, the maximum the facility can handle.

$$P_{coal} = P_{coal,nominal} \frac{\dot{M}_{coal,new}}{\dot{M}_{coal,nominal}} \tag{3}$$

3.2. Rotary Kiln

Energy and mass balances of the rotary kiln stone, air, and brick are used to model the calcination process.

3.2.1. Air

The air is assumed to be well mixed and only vary down the length of the kiln.

Coal Combustion

Combustion of coal generates the required heat for calcination. Coal particles are fired and combusted down the length of the rotary kiln. The kinetics and heat released by the combustion are described by Mujumdar (Mujumdar *et al.* , 2006).

The mass combustion rate of coal is:

$$\dot{m}_{coal,rxn} = C_{coal,rxn}\rho_c^{2/3} v_{coal}^{-1/3} C_{O_2} \tag{4}$$

The reaction constant $C_{coal,rxn}$ is:

$$C_{coal,rxn} = MW_{coal} N p_{coal} k_{coal} x 4\pi \left(\frac{3A_g}{4Np_{coal}\rho_{coal}\pi}\right)^{2/3} \tag{5}$$

Equation 6 shows how the number of coal particles, Np_{coal}, is arrived at:

$$Np_{coal} = \frac{\dot{m}_{coal}}{\rho_{coal} V_{coal_P}} \tag{6}$$

The freeboard area, A_g, is described by Equation 7:

$$A_g = r_i^2 \pi (1 - \mathfrak{f}) \tag{7}$$

The fill, $\mathfrak{f}$, describes how full the kiln is with stone. Equation 8 is used to calculate the carbon particle density in the air, ρ_c:

$$\rho_c = \frac{\dot{m}_{coal}}{A_g v_{coal}} \tag{8}$$

The velocity of the particles down the length of the kiln, v_{coal}, is described by Equation 9.

$$v_{coal} = v_{coal_0} e^{-0.06x} \tag{9}$$

Finally, the concentration of oxygen, C_{O_2}, is calculated based on a mass balance down the length of the kiln assuming that coal combustion occurs as follows:

$$C(s) + O_2(g) \rightarrow CO_2(g) \tag{10}$$

Due to the relatively high velocity of the air compared to the stones, the air is approximated to be at steady state conditions. Therefore the concentration of oxygen down the length of the kiln, C_{O_2}, is calculated as:

$$C_{O_2} = C_{O_{2_{in}}} - \frac{\int \dot{m}_{coal,rxn} dx}{MW_{coal}} \tag{11}$$

This generates the pseudo steady state oxygen profile down the length of the kiln.

Air Mass Balance

Regarding specific chemical species in air, only the concentration of oxygen was modelled in this simulation. The bulk flow of air in the rotary kiln was tracked for the total mass and total moles. Th air mass primarily comes from external air pulled through by the facility fans. However, gaseous components are added from the combustion of coal as well as the calcination of limestone to lime that generates carbon dioxide as shown respectively in Equation 10 and 1. As was done with the oxygen, the pseudo steady-state approximation was applied to the total moles and mass of the air.

Equation 12 describes the air mass balance for the system:

$$\dot{m}_{air} = \dot{m}_{air_{in}} + \int \dot{m}_{coal,rxn} dx + \int \dot{m}_{calc} dx \tag{12}$$

where $\dot{m}_{coal,rxn}$ and $\dot{m}_{calc}$ are, respectfully, the mass generated from the coal combustion and calcination of limestone. x describes the longitudinal direction down the kiln. A similar balance is carried out for the moles of gas in the kiln as a function of the length in Equation 13. Notably, only the calcination reaction adds moles to the system.

$$\dot{n}_{air} = \dot{n}_{air_{in}} + \int \dot{n}_{calc} dx \tag{13}$$

Subsequently, the ideal gas law is employed using the number of moles to estimate the density of air, ρ_{air}. Based on facility information, the pressure in the kiln is atmospheric. Information about the air density enables a calculation of the air volumetric flow rate, $\dot{V}_{air}$ in Equation 14, as well as the air velocity, $\dot{v}_{air}$, when the volumetric flow rate is divided by the freeboard area in Equation 15.

$$\dot{V}_{air} = \frac{\dot{m}_{air}}{\rho_{air}} \tag{14}$$

$$\dot{v}_{air} = \frac{\dot{V}_{air}}{A_g} \tag{15}$$

Air Energy Balance

Calcination is a highly endothermic process (-1800 kJ/(kg limestone)) (Georgallis, 2004). Therefore, high heat transfer from the air to the stones is critical to support the calcination. Energy is added to the air from the combustion of coal and then transferred to the stone. Equation 16 is the air energy balance in the kiln.

$$\rho_{air}\pi ri^2(1-\text{f})C_{p,air}\frac{\partial T_{air}}{\partial t} = adv_{air} - conv_{a\to s} - rad_{a\to s} - conv_{a\to b} - rad_{a\to b} + coal_{comb} \tag{16}$$

where the advective term, adv_{air}, is:

$$adv_{air} = C_{p,air}\frac{\partial(\dot{m}_{air}T_{air})}{\partial x} \tag{17}$$

The convective heat transfer from air to stone, $conv_{a\to s}$, is:

$$conv_{a\to s} = h_{a\to s}P_{stone}(T_{air} - T_{stone}) \tag{18}$$

The radiative heat transfer from air to stone, $rad_{a\to s}$, is:

$$rad_{a\to s} = \epsilon_{CO_2}\sigma P_{stone}(T_{air}^4 - T_{stone}^4) \tag{19}$$

The convective heat transfer from air to brick, $conv_{a\to b}$, is:

$$conv_{a\to b} = h_{a\to b}P_{brick}(T_{air} - T_{brick}) \tag{20}$$

The radiative heat transfer from air to brick, $rad_{a\to b}$, is:

$$rad_{a\to b} = \epsilon_{CO_2}\sigma P_{brick}(T_{air}^4 - T_{brick}^4) \tag{21}$$

The coal combustion, $Coal_{comb}$, is:

$$Coal_{comb} = \dot{m}_{coal,rxn}H_{coal} \tag{22}$$

where P_{stone} is the perimeter of the stone in contact with the freeboard air, shown in Figure 3. The P_{brick} is the perimeter of the brick contacting the freeboard air, also shown in Figure 3.

The Nusselt heat transfer correlation from the air to the stone and air to brick to find the heat transfer coefficients comes from Li (Li *et al.* , 2005). The Nusselt correlation for air to stone is:

$$Nu_{a\to s} = 0.46 Re_{air}^{0.535} Re_w^{0.104} \mathfrak{f}^{-0.341} \tag{23}$$

The Nusselt correlation for air to brick is:

$$Nu_{a\to b} = 1.54 Re_{air}^{0.575} Re_w^{-0.292} \tag{24}$$

where Re_{air} is the Reynolds number for air and Re_w is the rotational Reynolds number calculated using the following formula:

$$Re_w = \frac{De^2 w}{\mu \rho_{air}} \tag{25}$$

where De is the an effective diameter of the freeboard area:

$$De = r_i \frac{(2\pi - \theta/2 + sin(\theta/2)}{\pi - \theta/4 + sin(\theta/4)} \tag{26}$$

where θ is the interior angle of the fill as shown in Figure 3.

Mixing plays a critical role in spreading heat throughout the stone in the rotary kiln bed. Ferron identified fill as inversely proportional to the mixing rate and Finnie identified rotation rate as proportional to the mixing rate (Ferron & Singh, 1991; Finnie *et al.* , 2005). Therefore, an additional penalty term to the heat transfer from the air to stone was used to. A modified form of the mixing index from Finnie was used to generate the term (Finnie *et al.* , 2005).

$$mixing\, penalty = 1 - e^{\frac{-Cw}{\mathfrak{f}}} \tag{27}$$

3.2.2. Stone

Outside of the imposition of the heat transfer penalty, the stone is assumed to be well mixed and only vary down the length of the kiln.

Stone Mass Balance

The mass of stone is tracked with two components, the total bulk volume of stone and the radius of limestone. As the reaction shown in Equation 1 proceeds, the limestone core continues to shrink and becomes lime, as shown in Figure 4. As a result, the volume of the stone is preserved, while the density changes. The bulk volume balance of the stone is:

$$\frac{\partial V_{stone}}{\partial t} = \pi r_i^2 v_{stone} \frac{\partial \mathfrak{f}}{\partial x} \tag{28}$$

The mass flow rate of stone out of the kiln is:

$$\dot{m}_{stone,out} = \mathfrak{f}_{end} v_{stone} \rho_{stone} \tag{29}$$

where the stone velocity, v_{stone}, is approximated from Perron and Bui as (Perron & Bui, 1990):

$$v_{stone} = \frac{r_i w sin(\alpha)}{sin(\beta)\sqrt{1 - \frac{sin^2(\alpha)}{sin^2(\beta)}}} \tag{30}$$

α is estimated to be 37.7^o (Liu *et al.* , 2005). The kinetics of the shrinking core reaction are used to track radius of the limestone, inside of individual stones, down. According to Ar, the kinetics of limestone to lime conversion is a zeroth order reaction (Ar & Doğu, 2001). The radial rate at which the stone core of limestone shrinks is:

$$\dot{r}_{LS,rxn} = \frac{MW_{LS} k_s}{\rho_{LS}} \tag{31}$$

where the kinetic rate constant, k_s, is only a function of temperature:

$$k_s = k_{s0} e^{\frac{Ea_{LS}}{RT_{stone}}} \tag{32}$$

The total number of calcined moles, $\dot{n}_{calc}$, can then be calculated:

$$\dot{n}_{calc} = \frac{3V_{stone}}{r_{stone}^3} r_{LS}^2 \dot{r}_{LS,rxn} \frac{\rho_{LS}}{MW_{LS}} \tag{33}$$

The average limestone radius for the stones down the length of the kiln is described by the following differential equation:

$$\frac{\partial r_{LS}}{\partial t} = \frac{v_{stone} \frac{\partial r_{LS}^3}{\partial x} - r_{LS}^3 \frac{\partial V_{stone}}{\partial t}}{3V_{stone} r_{LS}^2} - \dot{r}_{LS,rxn} \tag{34}$$

From the limestone radius, the mass conversion can be extrapolated as:

$$conv = 1 - \frac{r_{LS} \rho_{LS}}{r_{LS}^3 \rho_{LS} + (r_{stone}^3 - r_{LS}^3)\rho_L} \tag{35}$$

Stone Energy Balance

The energy balance for the stone is similar to that of the air; however, the heat transfer between the stone and the wall is considered negligible. The energy into the stone is driven by heat transfer from the air and energy loss comes from the highly endothermic reaction.

$$\rho_{stone} V_{stone} C_{p,stone} \frac{\partial T_{stone}}{\partial t} = adv_{stone} + conv_{a \to s} + rad_{a \to s} + \dot{n}_{calc} H_{calc} \tag{36}$$

where the stone advective term, adv_{stone}, is:

$$adv_{stone} = C_{p,stone} \frac{\partial (V_{stone} T_{stone} \rho_{stone})}{\partial x} \tag{37}$$

The density of the stone is a weighted average of the density of lime and limestone, based on the composition. The molecular weight of lime is 56 kg/kmol and the molecular weight of limestone is 100 kg/kmol.

3.2.3. Brick

Brick Energy Balance

The temperature of the brick is estimated to change in the radial and longitudinal direction of the kiln. Equation 38 describes the heat equation for the brick with diffusive heat transfer.

$$\rho C_{p,brick} \frac{\partial T_{brick}}{\partial t} = \frac{k_{brick}}{r} \frac{\partial}{\partial r} \left(r \frac{\partial T_{brick}}{\partial r} \right) + k_{brick} \frac{\partial^2 T_{brick}}{\partial x^2} \tag{38}$$

On the boundaries of the kiln, the heat is transferred convectively and radiatively. On the inside, hot air transfers heat to the brick shown in Equation 20 and 21. On the outside heat is convectively transfered from the kiln to the ambient air:

$$conv_{brick \to amb} = h_0 P_{kiln} (T_{brick} - T_{amb}) \tag{39}$$

Radiative heat transfer also occurs from the kiln to the ambient air through a sheet of steel that lines the rotary kiln. Steel emissivity is used to estimate heat loss via radiation.

$$rad_{brick \to amb} = \epsilon_{steel} P_{kiln} (T_{brick3}^4 - T_{amb}^4) \tag{40}$$

3.3. Pre-heater and cooler

The stone pre-heater and stone cooler were modelled in the same manner as the rotary kiln. The key distinction was the use of a constant heat transfer coefficient, $h_{ph/c}$, instead of one based on the rotation rate and fill of the kiln. This was done since the stones were approximated to be still. Also, it was assumed that no calcination occurred outside of the kiln.

3.4. Numerical Methods

This model was simulated using the ODE23s solver in Simulink. The partial differential equations (PDEs) were spatially discretized to convert them to ordinary differential equations (ODEs). The ODEs are compatible with the selected solver. A segment of longitudinally discretized kiln is illustrated in Figure 5.

Discretized Brick Energy Balance

An example of the discretization with the brick energy balance is shown in Figure 6. The brick energy balance PDEs varied in the radial direction, in the longitudinal direction, and in time. The radial and longitudinal directions were discretized to finite differences. Therefore, the brick was modelled as having three separate layers in the radial direction, as shown in Figure 6, and 50 separate layers in the longitudinal direction, 3 of which are shown in Figure 5. The longitudinal direction layer of interest is generalized to subscript i.

Inside layer

$$\frac{dT_{brick1}}{dt} = \frac{conv_{a,i\to b1,i} + rad_{a,i\to b1,i} + diff_{b1,i\to b2,i} + diff_{b1,i-1\to b1,i} - diff_{b1,i\to b1,i+1}}{\rho_{brick} C_{p,brick} \pi((ri+\Delta r)^2 - ri^2)\Delta x} \tag{41}$$

Middle layer

$$\frac{dT_{brick2}}{dt} = \frac{-diff_{b1,i\to b2,i} + diff_{b2,i\to b3,i} + diff_{b2,i-1\to b2,i} - diff_{b2,i\to b2,i+1}}{\rho_{brick} C_{p,brick} \pi((ri+2\Delta r)^2 - (ri+\Delta r)^2)\Delta x} \tag{42}$$

Outside layer

$$\frac{dT_{brick3}}{dt} = \frac{-diff_{b2,i\to b3,i} - conv_{b3,i\to amb,i} - rad_{b3,i\to amb,i} + diff_{b3,i-1\to b3,i} - diff_{b3,i\to b3,i+1}}{\rho_{brick} C_{p,brick} \pi((ri+3\Delta r)^2 - (ri+2\Delta r)^2)\Delta x} \tag{43}$$

where the diffusion between brick layers one and two is:

$$diff_{b1,i\rightarrow b2,i} = \frac{k_{brick}(T_{brick2,i} - T_{brick1,i})2\pi(ri + \Delta r)\Delta x}{\Delta r} \tag{44}$$

The diffusion between longitudinal layers is:

$$diff_{b2,i\rightarrow b2,i+1} = \frac{k_{brick}(T_{brick2,i} - T_{brick2,i+1})\pi((ri + 2\Delta r)^2 - (ri + \Delta r)^2)}{\Delta x} \tag{45}$$

The convective heat transfer from the kiln to the ambient air is:

$$conv_{b3,i\rightarrow amb,i} = h_0 P_{kiln}(T_{brick3,i} - T_{amb,i}) \tag{46}$$

The radiative heat transfer from the kiln to the ambient air occurs from the sheet of steel that lines the rotary kiln. Steel emissivity is used to estimate heat loss through radiation.

$$rad_{b3,i\rightarrow amb,i} = \epsilon_{steel} P_{kiln}(T^4_{brick3,i} - T^4_{amb,i}) \tag{47}$$

3.5. Steady State Example Results

For the operation of the rotary kiln, the above model is employed to track critical properties of the kiln. Figures 7 through 11 show properties of the kiln operated at steady state with a coal feed rate of 6.8 kg/s, air flow of 80 m^3/s, a rotation rate of 0.1377 1/min, and stone feed rate of 21.05 kg/s. Figure 7 illustrates the conversion of limestone to lime down the length of the kiln. Figure 8 shows the stone, air, and interior brick temperatures as a function of the kiln length. Most of the conversion occurs in the kiln range from 40 to 80 meters in length, where the temperature is around 1400 K (1127 ^oC). However, all portions of the process are crucial to heat the stone up to the required temperature. Figure 9 shows the temperatures of the three brick layers as a function of the kiln length. The brick temperature figure demonstrates how useful the brick is in conserving energy inside of the kiln. Figure 10 shows the air and stone temperatures down the length of the cooler. Figure 11 shows the air and stone temperatures down the length of the pre-heater.

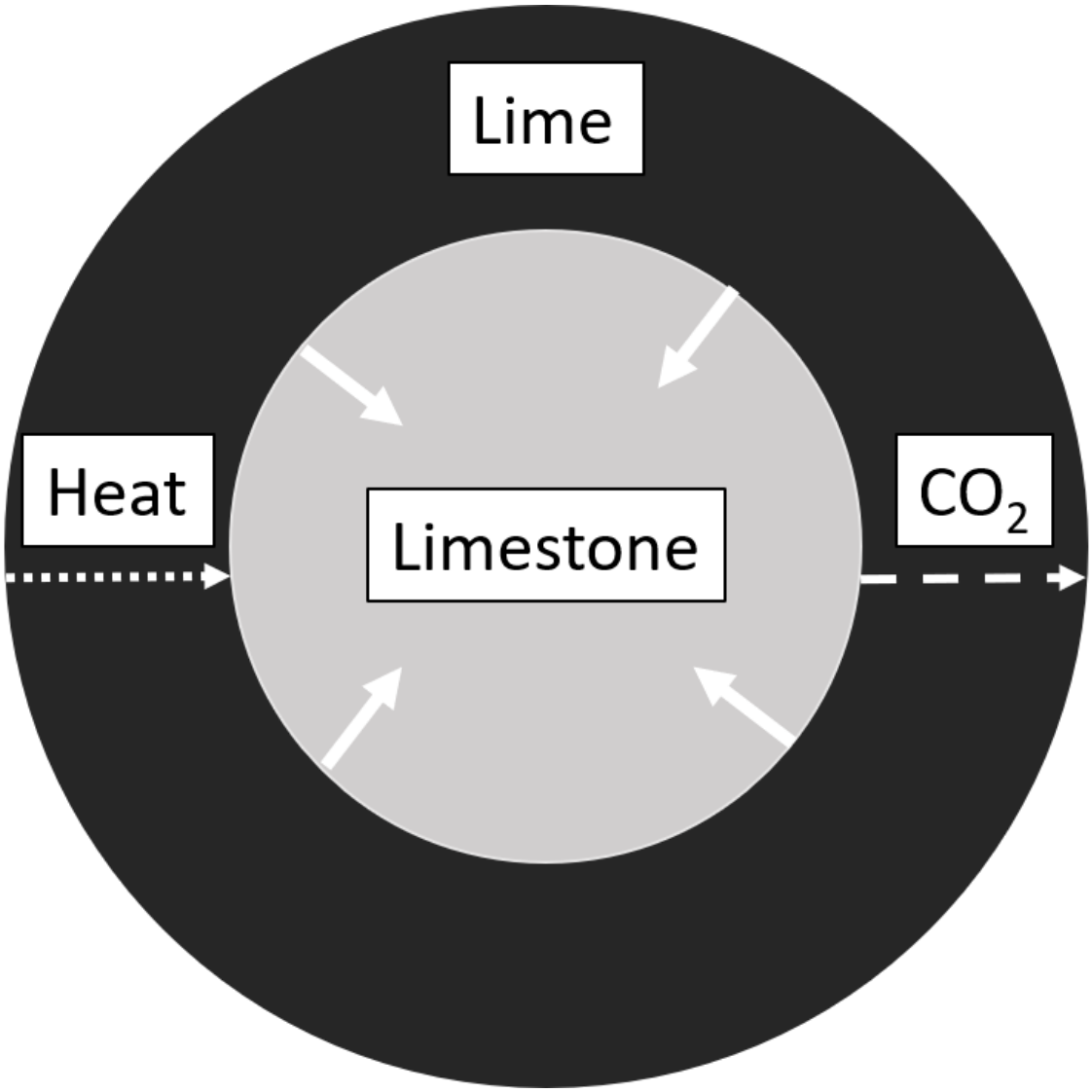

Figure 4: Shrinking core model for one limestone stone. Energy (heat) and mass (CO_2) transfer are illustrated.

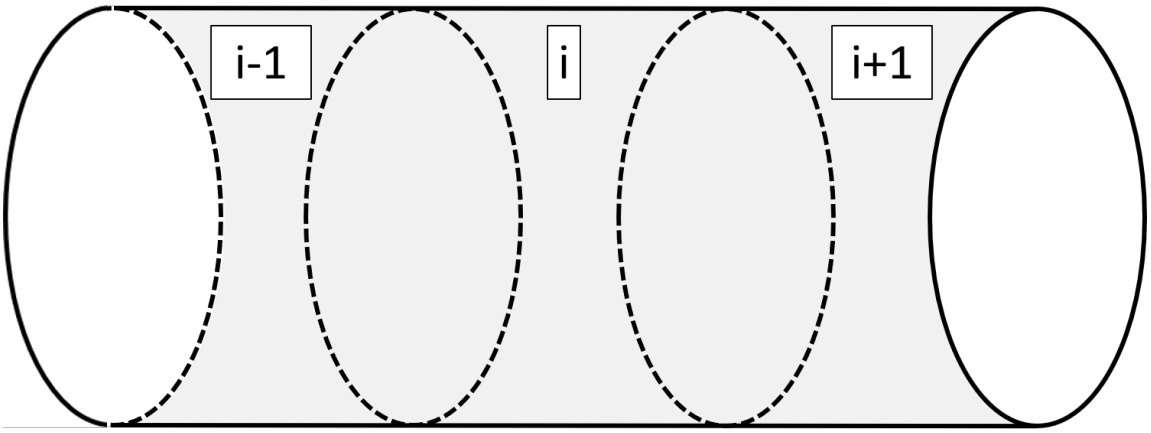

Figure 5: Small segment of discretized kiln in the longitudinal direction, used for mass and energy balances of stone and air. Only 3 (i-1, i, and i+1) of the 50 modelled segments are shown.

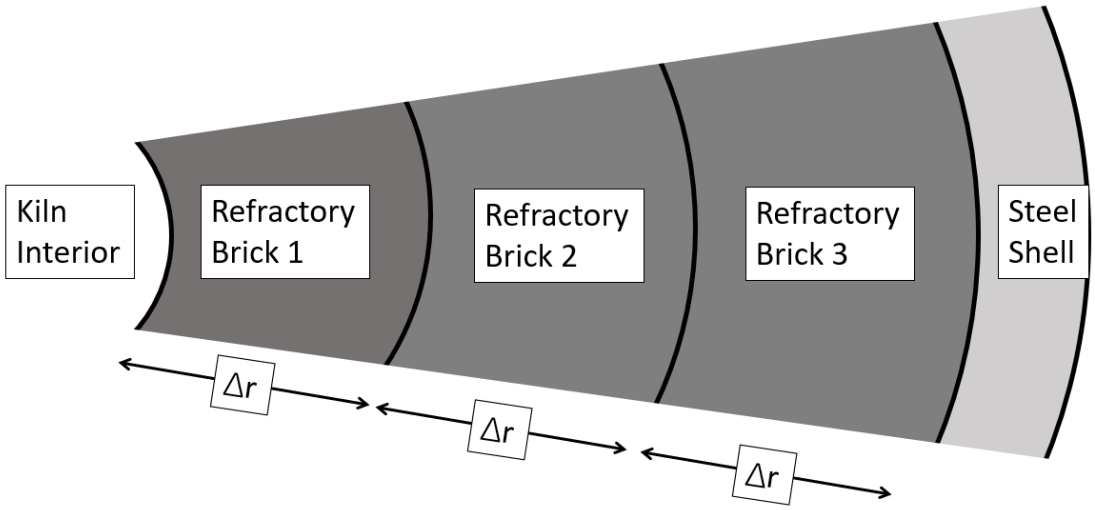

Figure 6: Discretized cross section of kiln brick.

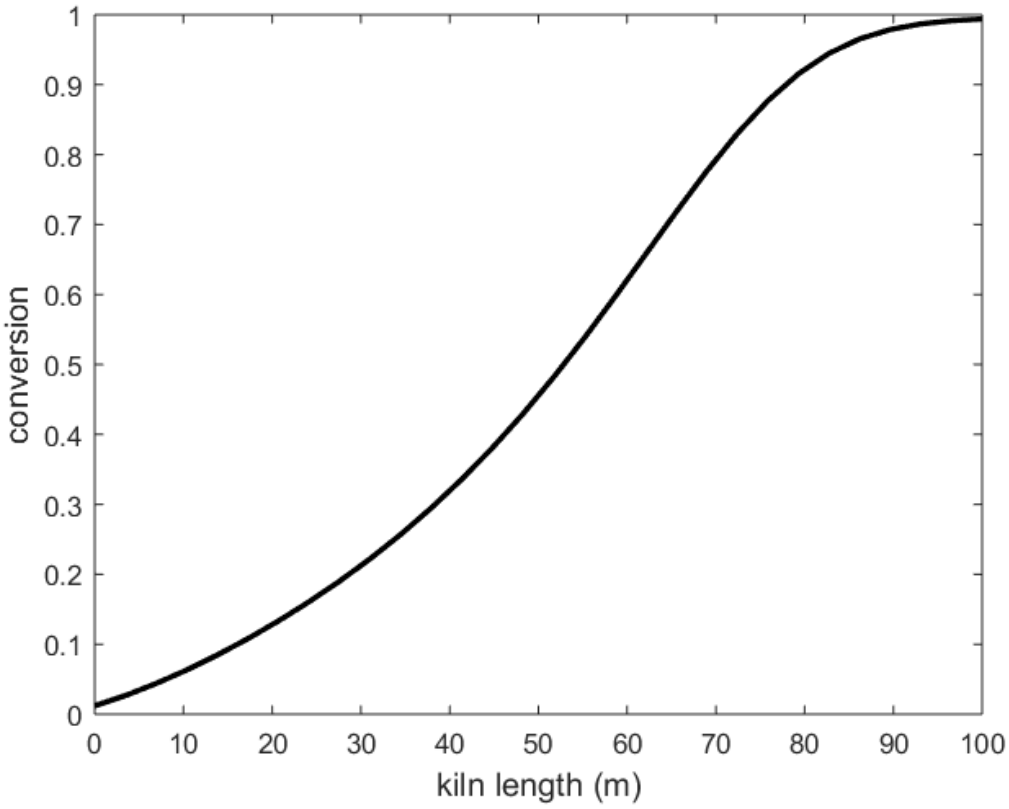

Figure 7: Conversion of limestone to lime as a function of kiln length for steady state, nominal operating conditions. Most of the conversion occurs in the heart of the kiln where the stone is sufficiently heated.

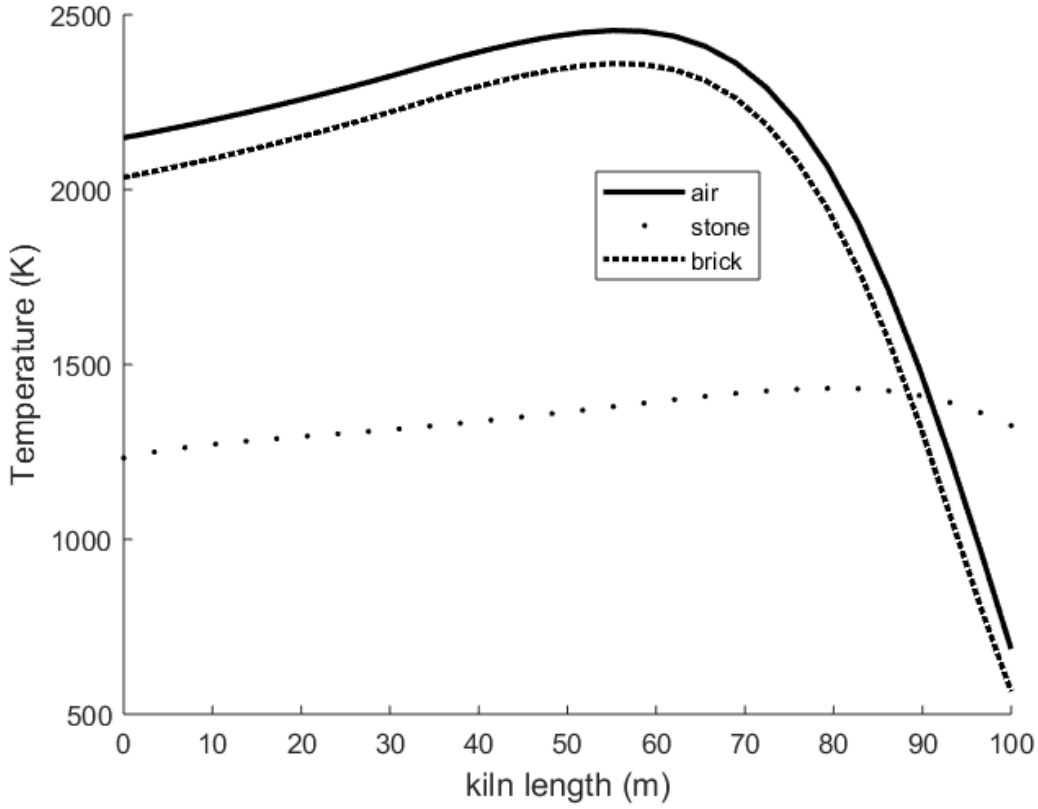

Figure 8: Air, stone, and interior brick temperature as a function of kiln length for steady state, nominal operating conditions.. The air and stone reach much higher temperatures than the stone. Most of the energy transferred to the stone drives the conversion of limestone to lime reaction.

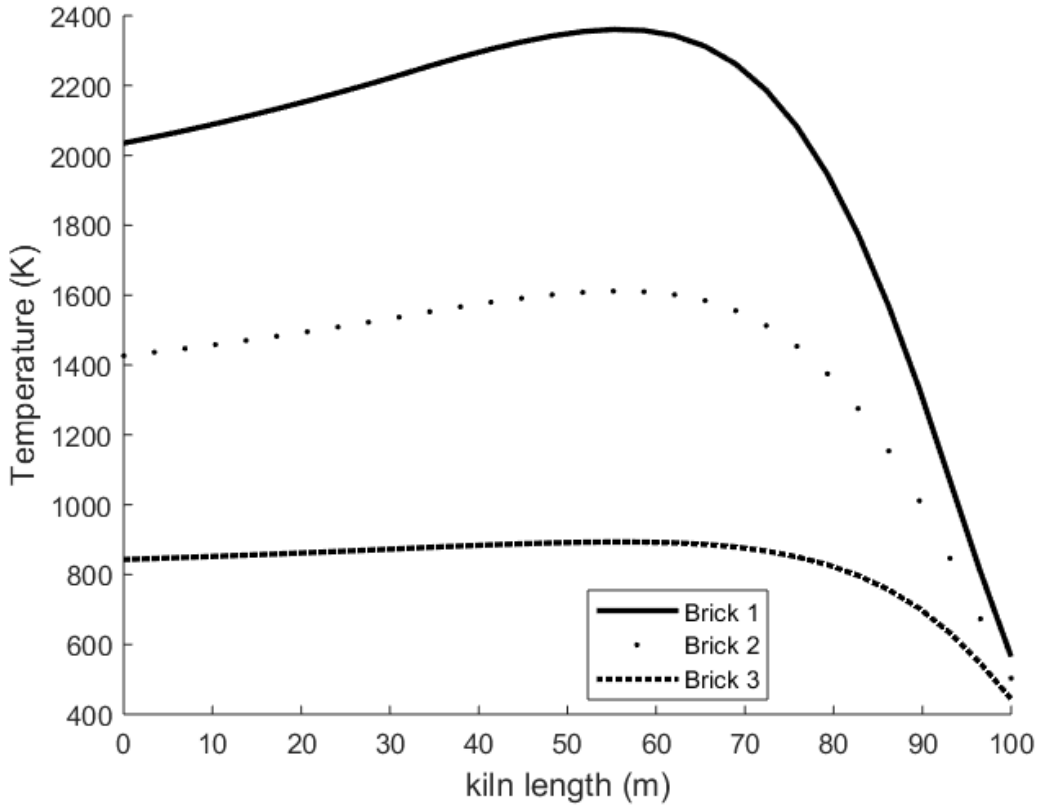

Figure 9: Kiln brick temperatures, for the interior (Brick 1), middle (Brick 2), and exterior layer (Brick 3) for steady state, nominal operating conditions.. The brick effectively keeps energy inside of the kiln.

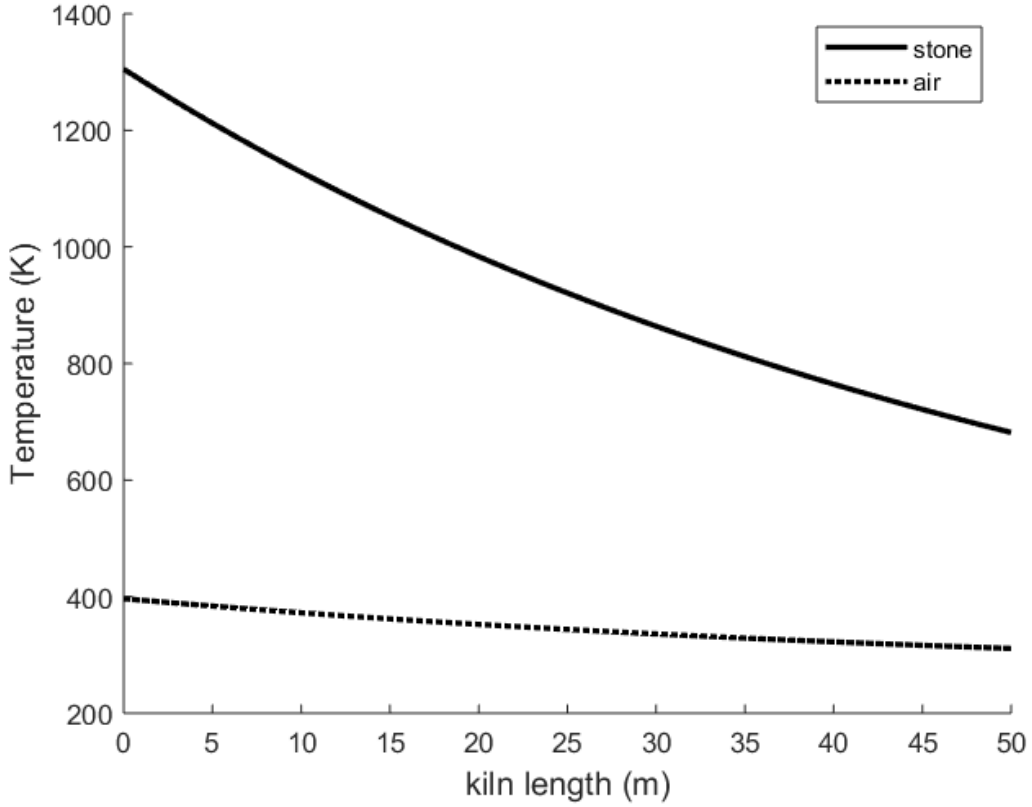

Figure 10: Stone and air temperatures down the length of the stone cooler for steady state, nominal operating conditions..

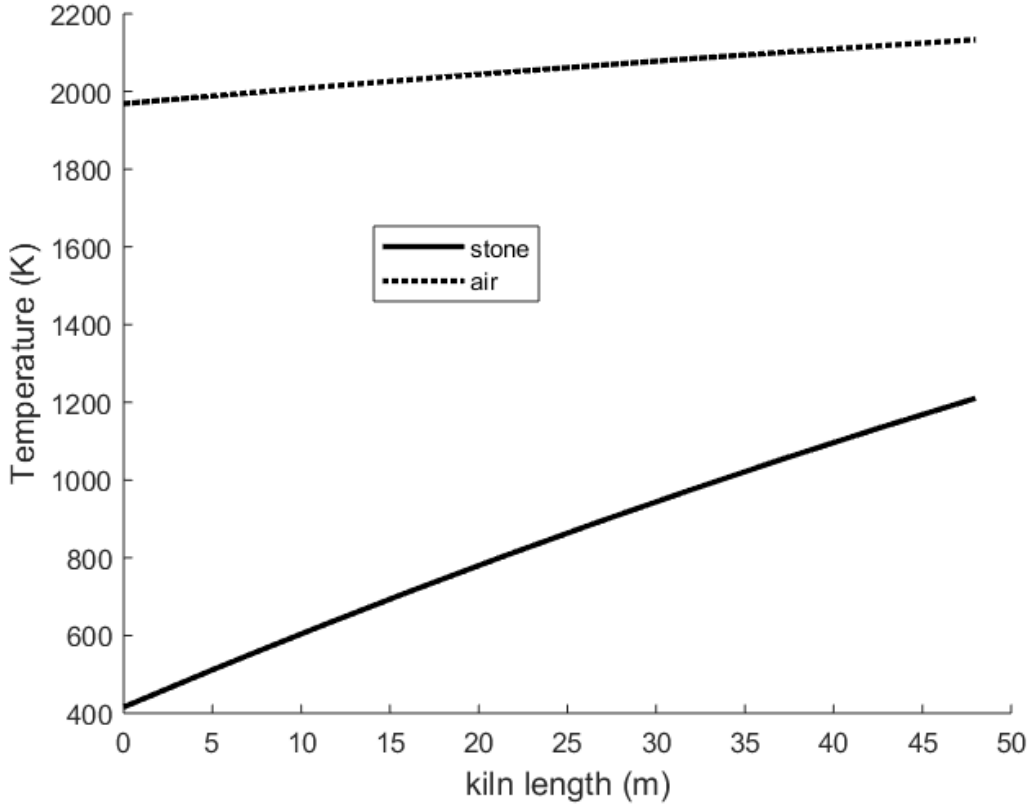

Figure 11: Stone and air temperatures down the length of the stone preheater for steady state, nominal operating conditions..

4. Results

4.1. Steady State Optimization

Although the core of this paper revolves around dynamic operation of a rotary kiln, it is necessary to first evaluate steady state optimization. Steady state optimization identifies baseline states of kiln operation from which the dynamic operation can deviate.

High air temperature is critical to achieving high conversion of limestone to lime in the rotary kiln. Of the four manipulated variables (coal feed rate, fan power, rotation rate, and stone feed rate), coal feed rate and fan power (air flow rate) determine the air temperature. Air temperature is directly proportional to coal feed rate, and inversely proportional to the air feed rate, therefore coal feed rate is maximized and air flow is minimized in order to maximize air temperature. This optimization is performed with the constraint that the air feed must contain at least a two percent excess of oxygen compared to the carbon in the coal to achieve full conversion and remain within safety constraints.

Additionally, the maximum coal feed rate to the kiln is 6.8 kg/s. The resultant minimum air flow to achieve a two percent excess oxygen out of the kiln is 80 m^3/s. These conditions provide the hottest kiln conditions. To perform a rapid electric demand response the fan power must be constrained to achieve a desired power draw. Two other fan flow rates are examined, 40 m^3/s and 120 m^3/s. For a flow rate of 120 m^3/s the coal feed rate to the kiln is still maximized to achieve the highest possible kiln air temperature. For a flow rate of 40 m^3/s, the coal feed rate is scaled back to 3.4 kg/s for safety concerns. These three coal and air feed rate scenarios are summarized in Table 1.

Table 1: Coal flow rates, air flow rates, and fan power consumption at three steady states.

State	Coal (kg/s)	Air Flow (m^3/s)	Total Fan Power (kW)	Figure
1	3.4	40	73	12
2	6.8	80	584	13
3	6.8	120	1972	14

For each scenario, the coal and air feed rates are fixed prior to optimization. Two additional degrees of freedom remain: the stone feed rate and kiln rotation rate. These degrees of freedom determine the residence time, mixing, and stone fill inside of the kiln. For each of the scenarios presented in Table 1, the optimal steady state rotation rate and stone feed were found to be a minimal needed for optimization as shown in Equation 48.

$$\begin{aligned} \min_{\omega, \dot{m}_{stone}} \quad & -L_c \dot{m}_{stone,out(>95\%L)} + LS_c \dot{m}_{stone} + E_c P_{use} + C_c M_{coal} \\ \text{s.t.} \quad & \textit{kiln physics section } 3 \\ & \omega \geq 0 \\ & \dot{m}_{stone} \geq 0 \end{aligned} \tag{48}$$

The objective function represents the negative profit for the facility. The profit function for the facility is the value of lime generated less the cost of limestone, electricity, and coal input. The optimization was done by performing a parameter sweep over the relevant inputs and subsequently following a gradient descent from the best point in the parameter sweep to a minimum. The contour plots and optimal conditions for each scenario listed in Table 1, are illustrated in Figures 12, 13, and 14.

4.2. Model Predictive Control - Dynamic Optimization

The steady state optimization illustrates three states encountered for rapid electric demand response: unconstrained fan operation, constrained low-power operation, and constrained high-power operation. While the previous optimization shows ideal steady state operation for a given fan constraint, it does not take into account the transition from one steady state to another.

When possible, the kiln and associated fan will operate in an unconstrained state. However, when a rapid electric demand response signal is requested by grid operators, the fan operation immediately changes, and as a result, the coal feed rate may also immediately change. This disturbance must be buffered by dynamically adjusting the stone feed rate and kiln rotation rate.

The objective function for the transition of the rotary kiln from one steady-state to the next is to ensure the threshold for the minimal conversion of lime is achieved. The minimum acceptable conversion is 95 percent. Therefore, in the optimization problem, a minimization of off specification material, for this transition is described by Equation 49. The only acceptable value for this objective function is 0, indicating that all stone coming out of the kiln is of high quality. Critically, this means that no resources need to be devoted to separating out lower grade lime products that exit the kiln during dynamic operation.

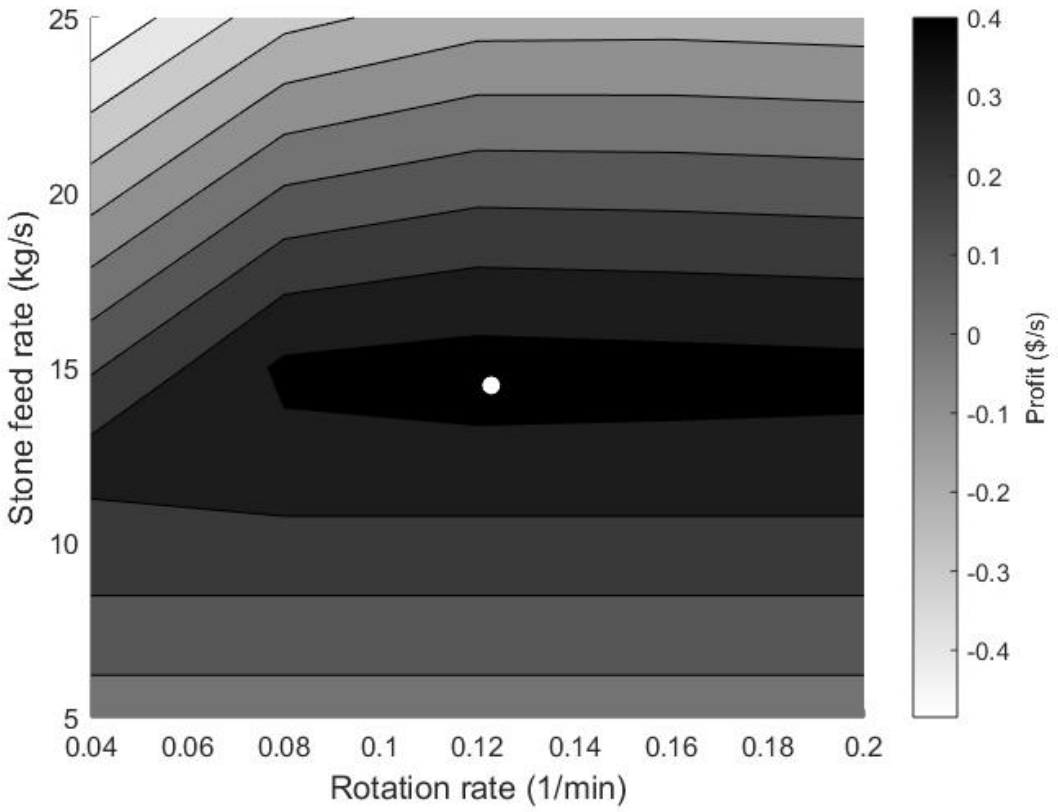

Figure 12: Contour plot of rotation rate and stone feed rate impact on rotary kiln profit rate with a coal feed rate of 3.4 kg/s and air flow rate of 40 m^3/s. The optimal conditions are shown by the white dot: rotation rate = 0.1288 1/min, stone feed rate = 14.48 kg/s, and profit of 0.4578 $/s.

$$\begin{aligned} \min_{\omega, \dot{m}_{stone}} \quad & \int max(0.95 - conv, 0)^2 dt \\ \text{s.t.} \quad & kiln\ physics\ section\ 3 \\ & \omega \geq 0 \\ & \dot{m}_{stone} \geq 0 \end{aligned} \tag{49}$$

Four electric grid regulation scenarios were explored: 1) Long-term transition to lower power 2) Long-term transition to high power 3) Short-term regulation down in power and 4) Short-term regulation up in power.

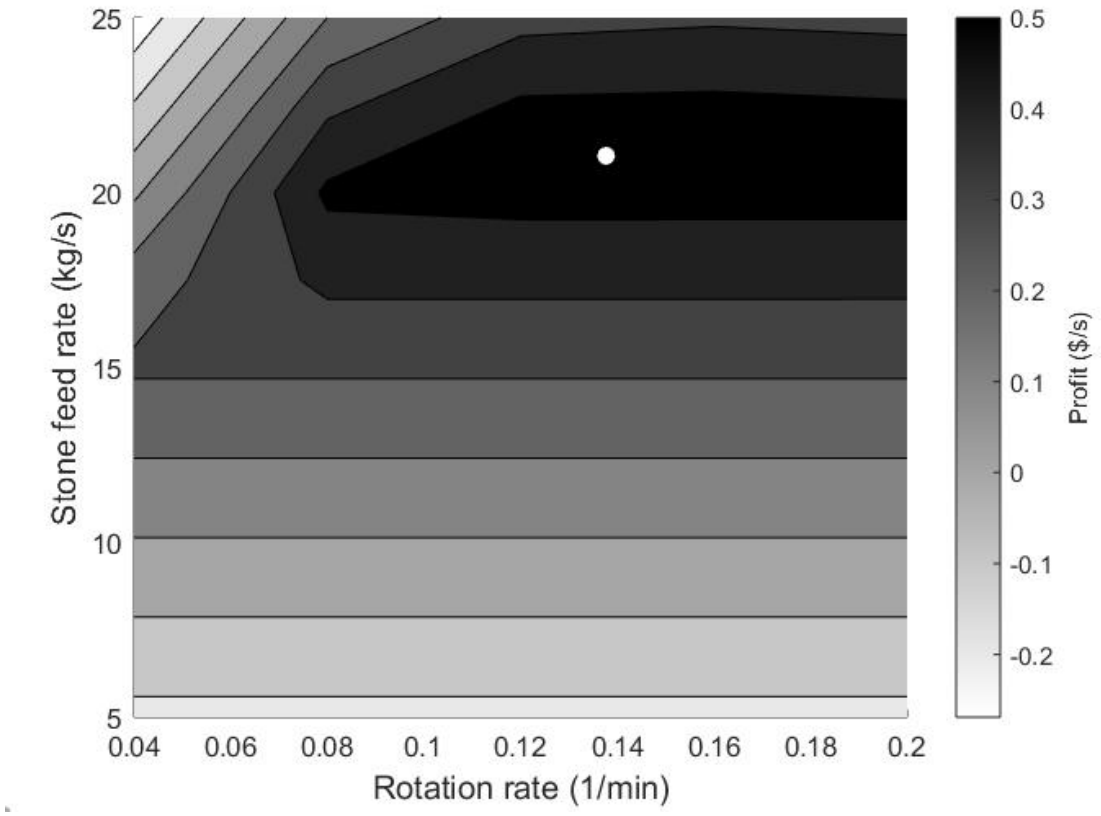

Figure 13: Contour plot of rotation rate and stone feed rate impact on rotary kiln profit rate with a coal feed rate of 6.8 kg/s and air flow rate of 80 m^3/s. The optimal conditions are shown by the white dot: rotation rate = 0.1377 1/min, stone feed rate = 21.05 kg/s, and profit of 0.5742 $/s.

Long-Term

Long-term transition to low power means decreasing the fan power from 584 kW to 73 kW. This decrease of over 0.5 MW of power consumption describes going from state 2 to state 1 of Table 1. Figure 15 demonstrates kiln properties for the transition. In the figures, the first vertical line indicates the time of the fan power disturbance, and the second horizontal line indicates the end of dynamic kiln operation. A naive response to this disturbance is to immediately operate the kiln at the new optimal steady state value. In the figure, this naive operation is juxtaposed against dynamic operation of the kiln using MPC.

The optimization problem is employed to parse out useful dynamic operation of the kiln. First, the time window for dynamic operation is selected, 1.5 hours for this

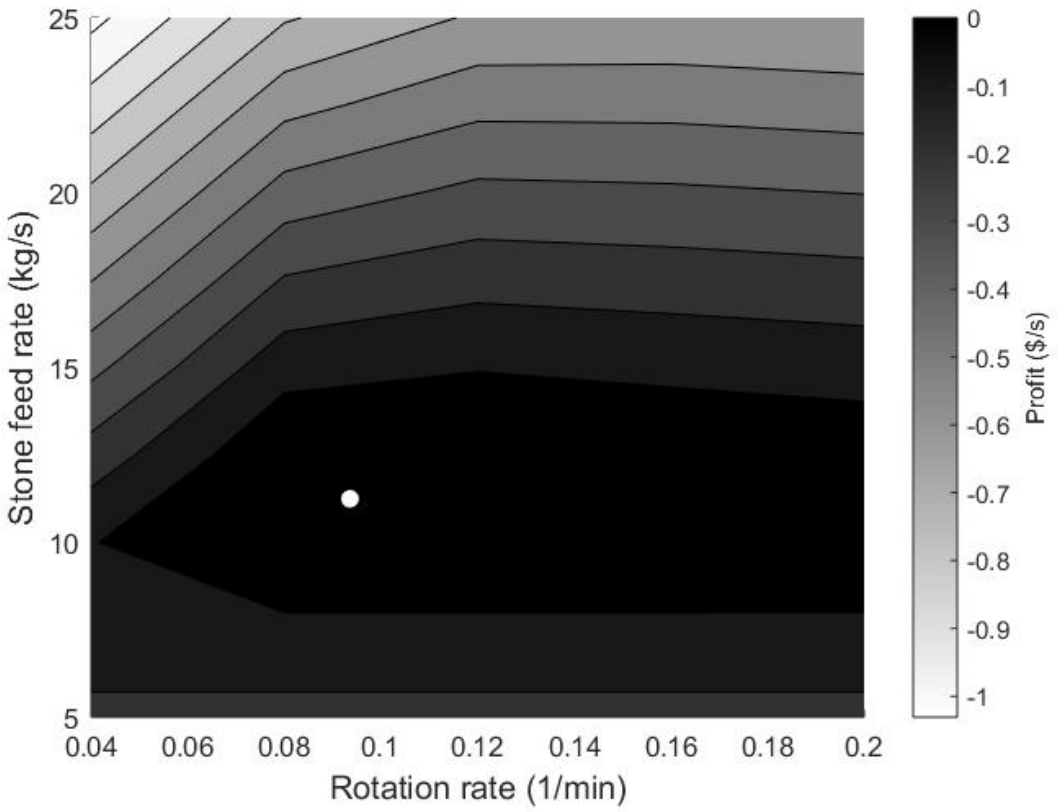

Figure 14: Contour plot of rotation rate and stone feed rate impact on rotary kiln profit rate with a coal feed rate of 6.8 kg/s and air flow rate of 120 m^3/s. The optimal conditions are shown by the white dot: rotation rate = 0.0936 1/min, stone feed rate = 11.24 kg/s, and profit of 0.1312 \$/s.

transition, and then it is cut up into three 30-minute subsections to allow additional flexibility in operation of the kiln rotation rate and stone feed rate. Then an initial guess is made for dynamic operation of the kiln during the transition. Since the transition goes from the maximum air temperature to a lower temperature, it is expected that a lower stone feed rate (less energy for the reaction) and slower operation (longer residence time) will be needed for the transition to maintain acceptable values for limestone conversion. From the starting guess, a modified stochastic gradient descent algorithm was used to reach operating conditions that minimized Equation 49. Due to the non-convex nature of the problem, a traditional gradient descent method was unable to satisfy the objective function.

The modified gradient descent takes a randomly sized step from a normal dis-

tribution for the rotation rate and stone feed rate for each subsection of dynamic operation to determine dynamic operation, runs the simulation, and evaluates the objective function. If the objective function is lower than the previous state, the new state is updated, otherwise a new random step is taken. With each iteration, as the objective function decreases so does the standard deviation of the randomly sampled step. This is repeated until the objective function reaches 0, indicating high quality product.

The resultant rotation rate and stone flow rates for this scenario are illustrated in the two center plots in Figure 15. The rotation rate follows a 'U-shape' where the rotation rate is stepped down and back up for the three intervals. This pattern is inverse to the stone feed rate.

The combination of dynamic rotation and stone feed rate creates an oscillation for the fill at the front end of the kiln, shown in the top right figure. This oscillation is significantly damped and delayed by the time it reaches the halfway point of the kiln, near where the kiln is hottest based on Figure 8. The stone temperature halfway down the kiln, illustrated in the bottom right figure, shows the resultant temperature spike that occurs when the reduced stone feed rate reaches the center of the kiln. As shown in the exit conversion plot, this MPC can maintain the conversion over the minimum acceptable limit. The profit rate is shown below the exit conversion. While the MPC and direct step both experience negative profit rates during the transitions, the losses experienced with the MPC transition are lower and briefer. Further, the conversion with the direct step change would require sorting low quality product, while the dynamically operated kiln product is high quality. Most importantly, this transition can free up 0.5 MW of down regulation for the grid.

Long-term transition to high power corresponds to increasing the fan power from 584 kW to 1972 kW. This increase in over 1 MW of power consumption describes going from state 2 to state 3 of Table 1. Figure 16 illustrates that MPC can be used to transition from one steady state to another in a stable manner. The same modified gradient descent method as the step down was used to find the rotation rate and stone flow during dynamic operation that optimized the objective function. In this case, the dynamic operating range was two hours and divided into six segments of 15, 15, 30, 30, 15, and 15 minutes. The same 'U-shape' for the rotation rate and inverted 'U-shape' for the stone feed rate was found to satisfy the objective. The midpoint stone temperature, bottom right figure, also follows the inverted 'U-shape', and the kiln gets very hot during the slowest rotation of the kiln. This allows for longer exposure to the hot air. The fill of the kiln, top right figure, is fluctuating at the inlet during dynamic operation, but experiences minor deviations in the center. This operation is juxtaposed to directly stepping kiln operation from one set of steady

state input parameters to the next.

Importantly, through dynamic operation, the exit conversion of the kiln can be maintained above 0.95 as shown in the top left figure. Again, this allows for continuous processing of the exiting stone without having to sort out lower quality stone. The profit loss, shown in the bottom left figure, in the transition from one steady state to the next is also shallower and briefer for the dynamic operation as compared to the direct step change in operation.

Notably, coming back to steady state operation with a coal feed rate of 6.8 kg/s and 80 m^3/s of air can be achieved through a direct step in operating conditions. This is the case because there is excess energy in the kiln with these conditions to perform the calcination reaction.

Short-term

The last two cases demonstrate successful long-term transition from one steady state to the next; however, it is often the case that short-term electricity up and down regulation is needed in ancillary services. For short-term electricity regulation, the MPC can anticipate that the kiln operation will rapidly return to the overall optimal operation (state 2 of Table 1). The knowledge of quickly returning to a hotter kiln air condition reduces the need for drastic dynamic operation. Instead, a short-term operation can be used to bridge operation between steady states.

Both up and down regulation of electricity consumption, short-term operation are examined. For kiln down regulation (reduced electricity consumption by 0.5 MW) a temporary transition is made from steady state. At steady state the kiln operates with the fans and coal described by state 2 of Table 1, then for an hour operate based on the coal and fan operation based on state 1, before returning to state 2. Conversely, naive operation manifests as operating based on the stone feed rate and rotation rate of state 2 of Table 1 (Figure 13), then jumping to full operation (including stone feed and rotation rate) of state 1 (Figure 12), and then returning to state two. However, the rotation rate and stone feed rate do not need to go to the new steady state to satisfy the objective function.

Instead, a gradient descent method is used to find the rotation rate and stone feed rate required to satisfy the limestone conversion limit. The initial guess to the objective function is the steady state operation based on state 2. Subsequently, the kiln rotation rate and stone feed rates are slowly lowered. Slower rotation means more exposure to hot kiln air, and less stone feed means less mass to heat up and react. Inching back these values slowly reduces the amount of off specification stone generated. This slow reduction is performed until all of the stone is of acceptable quality. Notably, many operating conditions will satisfy the objective function (i.e.

turning off the kiln), but this method still maximizes the amount of stone throughput by following the gradient descent.

Figure 17 shows the direct step operation of the kiln and the MPC of the kiln that satisfy the objective function for the one hour short-term dynamic operation during down regulation. The less drastic operation, compared to transitioning steady states, yields smoother results. The fill of stone in the kiln, top right subplot, never deviates outside of the 0.1 to 0.2 range. The stone temperature in the middle of the kiln, bottom right subplot, also stays close to 1200 K. Still, as shown by the exit conversion, top left subplot, these minor adjustments in operation from the nominal steady state keep all of the stone on specification standards. This is not the case with the naive operation. The profit rate is also only slightly reduced, compared to the negative profit rate from naive operation caused by output of low quality product. This demonstrates that it is reasonable for the kiln to perform short-term grid regulation services with only minor disruptions to the process. As the ancillary service time period is shortened, the impact on the process is further reduced.

The same study is carried out for a temporary regulation up (increase of 1 MW) in electricity consumption. Figure 18 shows the direct step operation of the kiln and the MPC of the kiln that satisfy the objective function for the two hour short-term operation during up regulation. This represent operation of fan air and coal flow from state 2 to state 3 and back to state 2 of Table 1. MPC control of the rotation rate and stone feed rate during the transition is compared to naive operation. The same gradient descent as the short-term down regulation was employed to find the MPC operating conditions. Neither the fill, top right subplot, nor stone temperature, bottom right subplot, deviate too much from steady state operation. However, the MPC slows down the operation more and reduces the stone feed rate more (compared to the down regulation), maintaining a higher stone temperatures, and avoiding the initial temperature dip experienced by the kiln with the direct step operation. The exit conversion, shown in the top left subplot, illustrates that high conversion can be maintained. Unfortunately, this optimal operation still results in a slightly negative profit. Fortunately, the negative profit rate is significantly less than the naive operation. Also, as the time period for short-term operation is reduced, higher stone feed rate and rotation rates can achieve acceptable conversion and will result in profitable operation. This shows how the facility can intelligently minimize downside and up regulate electricity consumption by 1 MW.

When in electric regulation mode, it is better for the kiln to operate in the short-term mode rather than to try and transition between steady states. Short-term transitional operation allows for less fluctuation and higher profit, but is only possible for short-term transitions. The long-term transitions are more useful when

there is no knowledge about how long the facility will be required to perform electric regulation or if the transition is for a very long time.

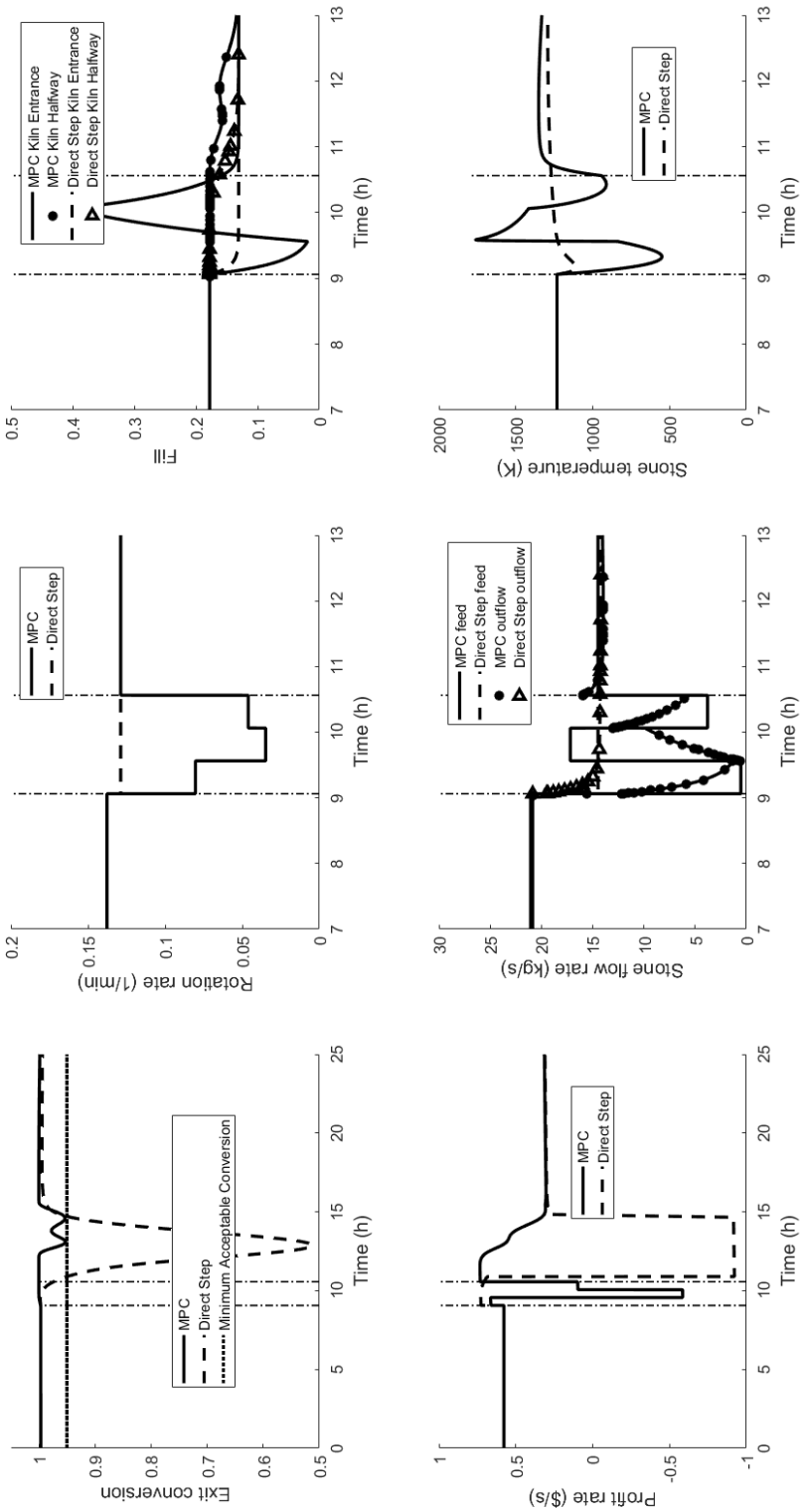

Figure 15: Rotary kiln metrics for long-term down regulation of power consumption (584 kW to 73 kW). From left to right the first row of subplots describes the limestone conversion, kiln rotation rate, and stone fill in the kiln. From left to right the second row of subplots describes the profit rate of the kiln, stone feed and stone out flow, and middle stone temperature in the kiln. The beginning of the disturbance is indicated by the first vertical dashed line, and the end of dynamic operation is indicated by the second vertical dashed line.

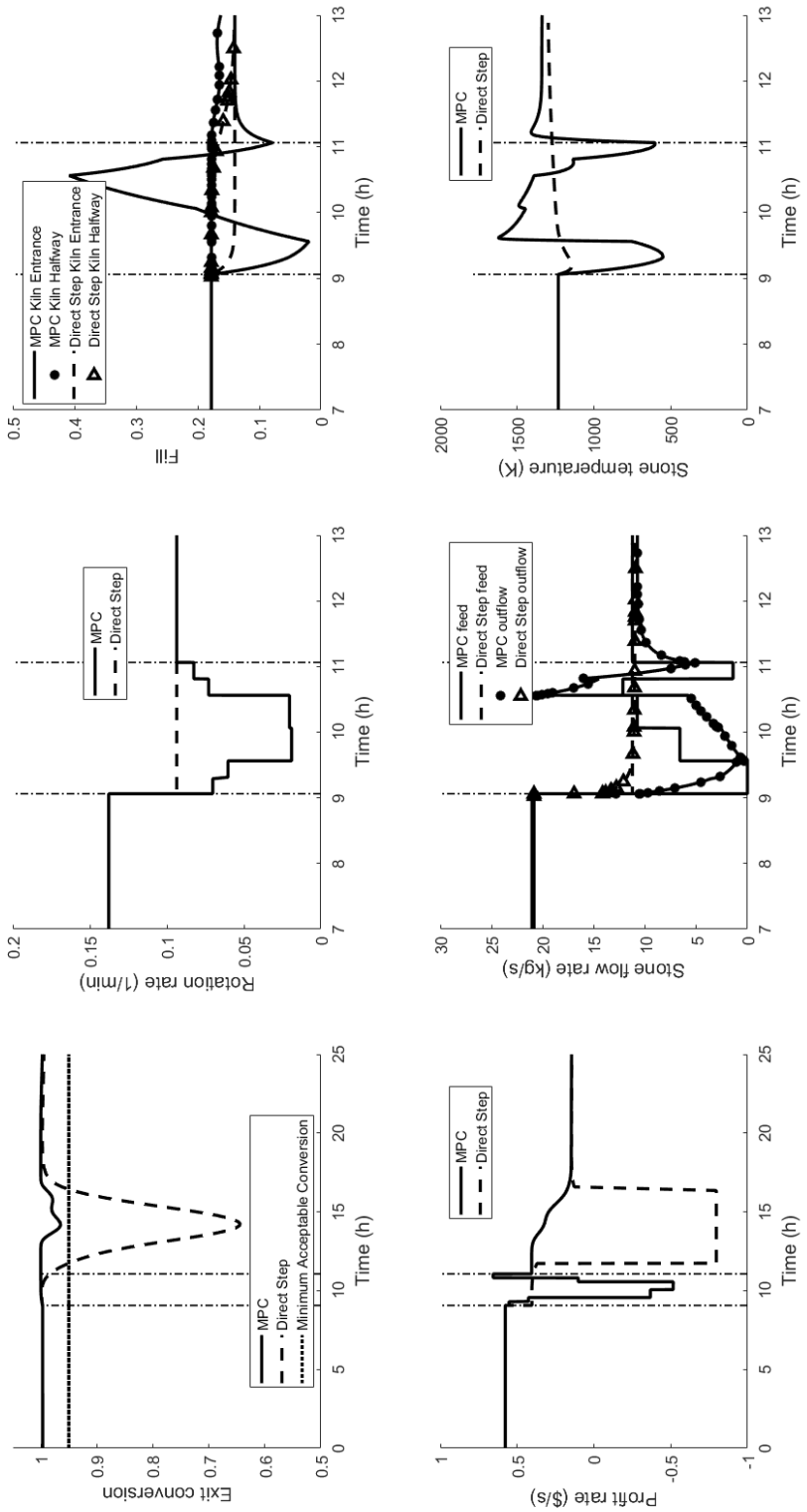

Figure 16: Rotary kiln metrics for long-term down regulation of power consumption (584 kW to 1972 kW). From left to right the first row of subplots describes the limestone conversion, kiln rotation rate, and stone fill in the kiln. From left to right the second row of subplots describes the profit rate of the kiln, stone feed and stone out flow, and middle stone temperature in the kiln. The beginning of the disturbance is indicated by the first vertical dashed line, and the end of dynamic operation is indicated by the second vertical dashed line.

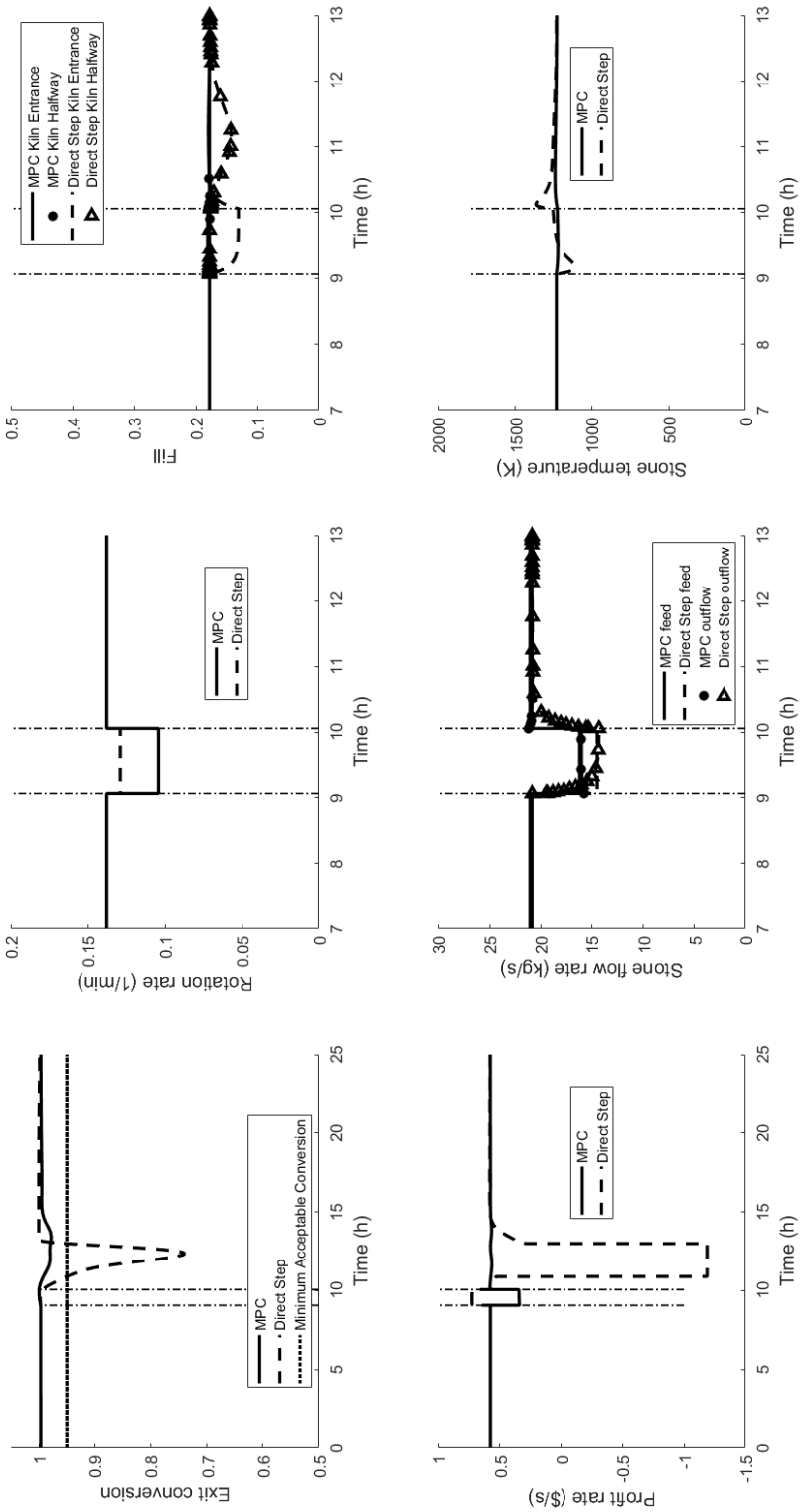

Figure 17: Rotary kiln metrics for temporary down regulation of power consumption (584 kW to 73 kW to 584 kW). From left to right the first row of subplots describes the limestone conversion, kiln rotation rate, and stone fill in the kiln. From left to right the second row of subplots describes the profit rate of the kiln, stone feed and stone out flow, and middle stone temperature in the kiln. The beginning of the disturbance is indicated by the first vertical dashed line, and the end of dynamic operation is indicated by the second vertical dashed line.

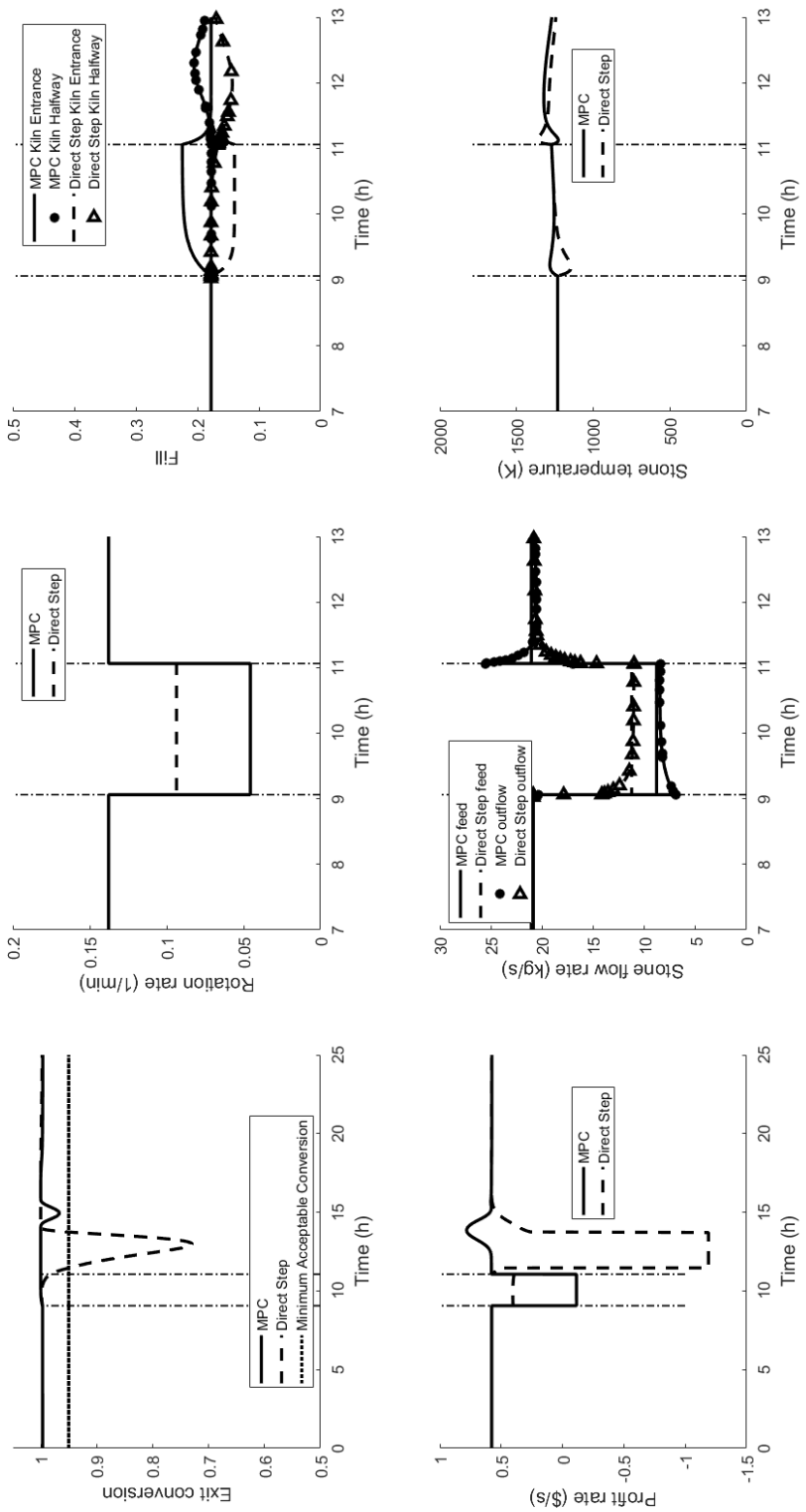

Figure 18: Rotary kiln metrics for temporary up regulation of power consumption (584 kW to 1972 kW to 584 kW). From left to right the first row of subplots describes the limestone conversion, kiln rotation rate, and stone fill in the kiln. From left to right the second row of subplots describes the profit rate of the kiln, stone feed and stone out flow, and stone temperature down in the kiln. The beginning of the disturbance is indicated by the first vertical dashed line, and the end of dynamic operation is indicated by the second vertical dashed line.

Summary

Table 2 summarizes the duration of poor quality stone production with direct step transitions for each of the four explored scenarios. Notably, MPC allows for that number to be reduced to a null value for all scenarios. The profits through the transitional regions of all scenarios for the direct step and MPC approaches is also displayed in Table 2. The transitional region is defined as starting from the air flow disturbance until the new steady state is reached. The profit from the MPC transition is always at least $12,600 greater than the direct step and turns the cumulative profit positive, despite having instantaneous points of profit loss. The steady-state profit in Table 2 shows the potential profit the kiln can make using the unconstrained steady-state optimum. The economic penalty of smart grid participation, not operating at steady-state, is reduced by at least 65% using MPC. For the short term participation, the reduction is at least 77%, increasing the prospect that the facility can be a valuable grid asset if they are appropriately compensated by grid operators.

Table 2: Summary poor limestone conversion in the direct step regime and transitional profit for the four explored ancillary service scenarios. The transitional region starts at the air flow rate disturbance and ends when the direct step methodology reaches the new steady state.

Scenario	Direct step poor quality duration (h)	Direct step transitional profit ($)	MPC transitional profit ($)	Steady-state profit ($)
Long-term up	4.7	-9,300	6,900	15,500
Long-term down	3.8	-7,700	9,700	12,600
Short-term up	2.3	-2,800	9,800	13,600
Short-term down	2.1	-1,700	11,000	12,600

5. Conclusion and Future Work

Rotary kilns, like other mineral processing equipment, are traditionally rigid and inflexible in their operation. However, this paper demonstrates that MPC can be leveraged for a rotary kiln facility to operate flexibly to perform ancillary services without reduction in product quality. The rotary kiln is able to increase power consumption by 1 MW and decrease power consumption by 0.5 MW. For short term participation, less than two hours, the economic penalty of participation is reduced by 77% using MPC. The dynamic operation readily handles all four explored scenarios (short and long-term increases and decreases in power consumption) to ensure product quality and minimize downside of the transitional operation. As is, deviations from optimal steady state operation are reflected negatively in the facility profit. However, this does not account for the positive economic pay out gained by performing the ancillary service as well as the environmental gains of increased renewable energy penetration.

The ease of MPC is increasing with cheaper sensors (to make models more reliable) and reduced computational expense. Simultaneously, the desire to increase renewable energy penetration into the grid is expanding. Both of these forces can catalyze the softening of rigid operation in mineral processing facilities. While this paper illustrates a single study of modified mineral processing, given a useful simulation, optimal dynamic operation with MPC can be applied to any mineral processing facilities. Specifically, this paper highlights how naive operation under an ancillary services regime is not feasible, but MPC provides a path for even rigid facilities, like the rotary kiln, to effectively participate in the smart grid.

Going forward, dynamic kiln operation optimization will focus not only on product quality assurance, but also profit maximization. This optimization will walk the delicate balance of maximizing throughput while still obliging ancillary service contracts and ensuring product quality. Additionally, a stochastic optimization analysis will be performed for short-term up and down regulation with unknown duration.

Acknowledgements

This research is funded by the U.S. Department of Energy Office of Energy Efficiency and Renewable Energy through the Industrial Assessment Centers program under grant # DE-EE0007712 and the Utah Governor's Office of Energy Development.

Competing Interest Statement

There were no competing interests in this research.

Nomenclature

Symbol	Description	Value (if constant)	Units
α	Angle of repose	37.7	deg
β	Angle of incline	1	deg
ϵ_{CO_2}	Emissivity of CO_2	0.01	–
ϵ_{Steel}	Emissivity of steel	0.08	–
θ	Interior angle of kiln	-	–
ρ_{brick}	Density of brick	3690	kg/m^3
ρ_c	Carbon particle density	-	$1/m^3$
ρ_{coal}	Density of coal	1346	kg/m^3
ρ_{LS}	Density of limestone	2300	kg/m^3
ρ_L	Density of lime	1288	kg/m^3
ρ_{stone}	Density of stone	-	kg/m^3
σ	Stefan-boltzmann constant	$5.67 * 10^{-11}$	$kW/m^2 - K^4$
ω	Rotation rate	-	$1/min$
Δx	Discretized longitudinal unit	2	m
Δr	Discretized radial unit	0.1	m
adv_{air}	Advective heat transfer of air	-	kW
adv_{stone}	Advective heat transfer of stone	-	kW
A_g	Freeboard area	-	m^2
C_c	Coal cost	0.05	$\$/kg$
$C_{coal_{rxn}}$	Coal reaction constant	-	–
C_{mix}	Mixing penalty	6	min
C_{O_2}	Concentration of oxygen	-	mol/m^3
$C_{O_2,in}$	Inlet concentration of oxygen	12.36	mol/m^3
$Coal_{comb}$	Heat from coal combustion	-	kW
$conv$	Conversion	-	–

Symbol	Description	Value (if constant)	Units
$conv_{a\to s}$	Convection from air to stone	-	kW
$conv_{a\to b1}$	Convection from air to internal brick	-	kW
$conv_{b3\to amb}$	Convection from external brick to ambient air	-	kW
$C_{p,air}$	Heat capacity of air	1	$kJ/kg-K$
$C_{p,brick}$	Heat capacity of brick	0.88	$kJ/kg-K$
$C_{p,stone}$	Heat capacity of stone	0.91	$kJ/kg-K$
De	Effective diameter of freeboard area	-	m
$diff_{b1\to b2}$	Diffusion from internal brick to central brick	-	kW
$diff_{b2\to b3}$	Diffusion from central brick to outside brick	-	kW
dr	Thickness of brick	0.05	m
E_c	Electricity cost	0.023	$\$/kWh$
Ea_{LS}	Activation energy of limestone	$1.56*10^2$	kJ/mol
$\mathfrak{f}$	Fill of stone in the kiln	-	$-$
$h_{a\to b}$	Heat transfer coefficient from air to brick	-	kW/m^2-K
$h_{a\to s}$	Heat transfer coefficient from air to stone	-	kW/m^2-K
h_0	Heat transfer coefficient from brick to ambient	0.001	kW/m^2-K
H_{calc}	Heat of calcination	1800	kJ/kg
H_{coal}	Heat of coal combustion	35,000	$kJ/kmol$
$h_{ph/c}$	Heat transfer coefficient in pre-heater or cooler	0.025	kW/m^2-K
k_{brick}	Diffusion coefficient of brick	0.0005	$kW/m-K$
k_{coal}	Kinetic coefficient of coal	-	m/s
k_s	Kinetic rate constant of limestone	-	$kmol/m^2-s$
k_{s0}	Nominal kinetic rate constant of limestone	0.419	$kmol/m^2-s$
L_c	Lime cost	0.13	$\$/kg$
LS_c	Limestone cost	0.04	$\$/kg$
$\dot{m}_{air}$	Mass flow rate of air	-	kg/s
$\dot{m}_{air_{in}}$	Mass flow rate of air into the kiln	-	kg/s
$\dot{m}_{calc}$	Mass flow from calcination	-	kg/s
$\dot{m}_{coal,rxn}$	Reaction rate of coal	-	kg/s
$\dot{m}_{coal,nominal}$	Nominal mass flow rate	-	kg/s
$\dot{m}_{stone}$	Stone feed rate	-	kg/s
MW_{coal}	Molecular weight of coal	12	$kg/kmol$
MW_L	Molecular weight of lime	100	$kg/kmol$
MW_{LS}	Molecular weight of limestone	56	$kg/kmol$
$\dot{n}_{air}$	Moles of air in the kiln	-	mol/s
$\dot{n}_{air_{in}}$	Moles of air into the kiln	-	mol/s
$\dot{n}_{calc}$	Moles of air generated from calcination	-	mol/s

Symbol	Description	Value (if constant)	Units
Np_{coal}	Number of coal particles	-	$-$
$Nu_{a\to s}$	Nusselt number for heat transfer air to stone	-	$-$
$Nu_{a\to b}$	Nusselt number for heat transfer air to brick	-	$-$
P_{brick}	Perimeter of brick touching the freeboard	-	m
P_{coal}	Coal crusher power	-	kW
$P_{coal_{nominal}}$	Nominal coal crusher power	140	kW
P_{fan}	Fan power	-	kW
$P_{fan_{nominal}}$	Nominal fan power	400	kW
P_{Kiln}	External perimeter of the kiln	19.6	m
P_{stone}	Perimeter of stone touching the freeboard	-	m
P_{use}	Power consumption	-	kWh/s
R	Ideal gas constant	8.314	$kJ/K-mol$
r_{stone}	Stone radius	0.051	m
$\dot{r}_{LC,reac}$	Radius shrinking rate of limestone	-	m/s
r_{LS}	Radius of limestone	-	m
$rad_{a\to b1}$	Radiative heat transfer air to internal brick	-	kW
$rad_{a\to s}$	Radiative heat transfer air to stone	-	kW
$rad_{b3\to amb}$	Radiative heat transfer external brick to ambient	-	kW
Re_{air}	Reynolds number of air	-	$-$
Re_w	Reynolds number of rotation	-	$-$
r_i	Interior radius of kiln	2.2	m
T_{air}	Air temperature	-	K
T_{amb}	Ambient temperature	-	K
T_{brick}	Brick temperature	-	K
T_{stone}	Stone temperature	-	K
$\dot{V}_{air}$	Air volumetric flow rate	-	m^3/s
v_{air}	Air velocity	-	m/s
$\dot{V}_{air_{nominal}}$	Nominal air volumetric flow rate	80	m^3/s
v_{coal}	Coal velocity	-	m/s
V_{coal_P}	Coal particle volume	$6.5 * 10^{-14}$	m^3
$v_{coal,0}$	Initial coal velocity	50	m/s
V_{stone}	Stone volume	-	m^3
v_{stone}	Stone velocity	-	m/s
x	Distance down kiln	-	m

6. References

Aghaei, Jamshid, & Alizadeh, Mohammad-Iman. 2013. Demand response in smart electricity grids equipped with renewable energy sources: A review. *Renewable and Sustainable Energy Reviews*, **18**, 64–72.

Alizadeh, MI, Moghaddam, M Parsa, Amjady, N, Siano, P, & Sheikh-El-Eslami, MK. 2016. Flexibility in future power systems with high renewable penetration: A review. *Renewable and Sustainable Energy Reviews*, **57**, 1186–1193.

Ar, Irfan, & Doğu, Gülşen. 2001. Calcination kinetics of high purity limestones. *Chemical Engineering Journal*, **83**(2), 131–137.

Barbour, Edward, Wilson, Grant, Hall, Peter, & Radcliffe, Jonathan. 2014. Can negative electricity prices encourage inefficient electrical energy storage devices? *International Journal of Environmental Studies*, **71**(6), 862–876.

Cambitsis, A. 2013. A framework to simplify the management of throughput and constraints. *Journal of the Southern African Institute of Mining and Metallurgy*, **113**(10), 769–773.

De Kock, Nicolaas Cornelius Jacobus Marthinus. 2006. *Researching the long-term impact of load management projects on South African Mines*. Ph.D. thesis, North-West University.

Faria, Pedro, & Vale, Zita. 2011. Demand response in electrical energy supply: An optimal real time pricing approach. *Energy*, **36**(8), 5374–5384.

Ferron, John R, & Singh, Dilip K. 1991. Rotary kiln transport processes. *AIChE journal*, **37**(5), 747–758.

Finnie, GJ, Kruyt, Nicolaas P, Ye, M, Zeilstra, C, & Kuipers, JAM. 2005. Longitudinal and transverse mixing in rotary kilns: A discrete element method approach. *Chemical Engineering Science*, **60**(15), 4083–4091.

Georgallis, Mike. 2004. *Mathematical modelling of lime kilns*. Ph.D. thesis, University of British Columbia.

Henning, Moriah, Machalek, Derek, & Powell, Kody M. 2019. Integrating a Microturbine into a Discrete Manufacturing Process with Combined Heat and Power Using Smart Scheduling and Automation. *Pages 293–298 of: Computer Aided Chemical Engineering*, vol. 47. Elsevier.

Holmberg, Kenneth, Kivikytö-Reponen, Päivi, Härkisaari, Pirita, Valtonen, Kati, & Erdemir, Ali. 2017. Global energy consumption due to friction and wear in the mining industry. *Tribology International*, **115**, 116–139.

Li, S-Q, Ma, L-B, Wan, W, & Yao, Q. 2005. A Mathematical Model of Heat Transfer in a Rotary Kiln Thermo-Reactor. *Chemical Engineering & Technology: Industrial Chemistry-Plant Equipment-Process Engineering-Biotechnology*, **28**(12), 1480–1489.

Lidbetter, Raine T, & Liebenberg, Leon. 2013. Load-shifting opportunities for typical cement plants. *Journal of Energy in Southern Africa*, **24**(1), 35–45.

Liu, Xiao Yan, Specht, E, & Mellmann, J. 2005. Experimental study of the lower and upper angles of repose of granular materials in rotating drums. *Powder Technology*, **154**(2-3), 125–131.

Ma, Ookie, Alkadi, Nasr, Cappers, Peter, Denholm, Paul, Dudley, Junqiao, Goli, Sasank, Hummon, Marissa, Kiliccote, Sila, MacDonald, Jason, Matson, Nance, *et al.* . 2013. Demand response for ancillary services. *IEEE Transactions on Smart Grid*, **4**(4), 1988–1995.

Mujumdar, Kaustubh S, Arora, Amit, & Ranade, Vivek V. 2006. Modeling of rotary cement kilns: applications to reduction in energy consumption. *Industrial & engineering chemistry research*, **45**(7), 2315–2330.

Njeng, AS Bongo, Vitu, Stéphane, Clausse, Marc, Dirion, J-L, & Debacq, Marie. 2015. Effect of lifter shape and operating parameters on the flow of materials in a pilot rotary kiln: Part II. Experimental hold-up and mean residence time modeling. *Powder technology*, **269**, 566–576.

Perron, Jean, & Bui, Rung-Tien. 1990. Rotary cylinders: solid transport prediction by dimensional and rheological analysis. *The Canadian Journal of Chemical Engineering*, **68**(1), 61–68.

Ping, Zhou, Xiang, Bo, & Tianyou, Chai. 2012. Improved disturbance observer (DOB) based advanced feedback control for optimal operation of a mineral grinding process. *Chinese Journal of Chemical Engineering*, **20**(6), 1206–1212.

Roberts, PD. 1979. An algorithm for steady-state system optimization and parameter estimation. *International Journal of Systems Science*, **10**(7), 719–734.

Rodríguez, José R, Pontt, Jorge, Newman, Patricio, Musalem, Rodrigo, Miranda, Hernán, Moran, Luis, & Alzamora, Gerardo. 2005. Technical evaluation and practical experience of high-power grinding mill drives in mining applications. *IEEE transactions on industry applications*, **41**(3), 866–874.

Sheha, Moataz N, & Powell, Kody M. 2018. Dynamic Real-Time Optimization of Air-Conditioning Systems in Residential Houses with a Battery Energy Storage under Different Electricity Pricing Structures. *Pages 2527–2532 of: Computer Aided Chemical Engineering*, vol. 44. Elsevier.

Sortomme, Eric, & El-Sharkawi, Mohamed A. 2012. Optimal scheduling of vehicle-to-grid energy and ancillary services. *IEEE Transactions on Smart Grid*, **3**(1), 351–359.

Sosa-Blanco, C, Hodouin, D, Bazin, C, Lara-Valenzuela, C, & Salazar, J. 1999. Integrated simulation of grinding and flotation application to a lead-silver ore. *Minerals Engineering*, **12**(8), 949–967.

Stebbins, Wayne L. 1994. Are you certain you understand the economics for applying ASD systems to centrifugal loads? *Pages 1–8 of: Proceedings of 1994 IEEE/IAS Annual Textile, Fiber and Film Industry Technical Conference*. IEEE.

Strbac, Goran. 2008. Demand side management: Benefits and challenges. *Energy policy*, **36**(12), 4419–4426.

Votteler, Roman Günter, & Brent, Alan Colin. 2016. A literature review on the potential of renewable electricity sources for mining operations in South Africa. *Journal of Energy in Southern Africa*, **27**(2), 1–21.

Westberg, B, Machalek, D, Denton, S, Sellers, D, & Powell, K. 2018. Proactive Automation of a Batch Manufacturer in a Smart Grid Environment. *Smart and Sustainable Manufacturing Systems*, **2**(2), 110–131.

Yang, Jun, Li, Shihua, Chen, Xisong, & Li, Qi. 2010. Disturbance rejection of ball mill grinding circuits using DOB and MPC. *Powder Technology*, **198**(2), 219–228.

Yu, Mengmeng, & Hong, Seung Ho. 2016. Supply–demand balancing for power management in smart grid: A Stackelberg game approach. *Applied energy*, **164**, 702–710.

Zhengyan, He, Zhang, Zhenyue, Junxia, YU, Zhigao, XU, *et al.* . 2016. Process optimization of rare earth and aluminum leaching from weathered crust elution-deposited rare earth ore with compound ammonium salts. *Journal of Rare Earths*, **34**(4), 413–419.